JHEP01(2016)155

Measurement of forward W and Z boson production in pp collisions at $\sqrt{s} = 8\,\text{TeV}$

The LHCb collaboration

E-mail: simone.bifani@cern.ch

ABSTRACT: Measurements are presented of electroweak boson production using data from pp collisions at a centre-of-mass energy of $\sqrt{s} = 8\,\text{TeV}$. The analysis is based on an integrated luminosity of $2.0\,\text{fb}^{-1}$ recorded with the LHCb detector. The bosons are identified in the $W \to \mu\nu$ and $Z \to \mu^+\mu^-$ decay channels. The cross-sections are measured for muons in the pseudorapidity range $2.0 < \eta < 4.5$, with transverse momenta $p_\text{T} > 20\,\text{GeV}/c$ and, in the case of the Z boson, a dimuon mass within $60 < M_{\mu^+\mu^-} < 120\,\text{GeV}/c^2$. The results are

$$\sigma_{W^+\to\mu^+\nu} = 1093.6 \pm 2.1 \pm 7.2 \pm 10.9 \pm 12.7\,\text{pb}\,,$$
$$\sigma_{W^-\to\mu^-\overline{\nu}} = 818.4 \pm 1.9 \pm 5.0 \pm 7.0 \pm 9.5\,\text{pb}\,,$$
$$\sigma_{Z\to\mu^+\mu^-} = 95.0 \pm 0.3 \pm 0.7 \pm 1.1 \pm 1.1\,\text{pb}\,,$$

where the first uncertainties are statistical, the second are systematic, the third are due to the knowledge of the LHC beam energy and the fourth are due to the luminosity determination. The evolution of the W and Z boson cross-sections with centre-of-mass energy is studied using previously reported measurements with $1.0\,\text{fb}^{-1}$ of data at $7\,\text{TeV}$. Differential distributions are also presented. Results are in good agreement with theoretical predictions at next-to-next-to-leading order in perturbative quantum chromodynamics.

Contents

1 Introduction

Measurements of W and Z boson production cross-sections at hadron colliders constitute important tests of the Standard Model (SM).[1] Theoretical predictions for these cross-sections are available at next-to-next-to-leading order (NNLO) in perturbative quantum chromodynamics [1–5]. The dominant uncertainty on these predictions reflects the uncertainties on the parton density functions (PDFs). The forward acceptance of the LHCb detector allows the PDFs to be constrained at Bjorken-x values down to 10^{-4} [6]. Ratios of the W and Z cross-sections provide precise tests of the SM as the sensitivity to the PDFs in the theoretical calculations is reduced and many of the experimental uncertainties cancel.

---

[1]Throughout this article Z is used to denote the Z/γ^* contributions.

During LHC Run 1, data were collected at centre-of-mass energies, $\sqrt{s}$, of 7 TeV and 8 TeV, providing two distinct samples for measurements of the electroweak boson production cross-sections. The evolution of the cross-sections, and cross-section ratios, may be used to infer the existence of physics beyond the Standard Model (BSM) [7].

LHCb has measured the W boson production cross-section at $\sqrt{s} = 7$ TeV using the muon channel [8], and that of Z bosons decaying to muon [9], electron [10] and tau lepton [11] pairs, using a data set of $1.0 \, \text{fb}^{-1}$. The Z boson production cross-section at $\sqrt{s} = 8$ TeV has also been measured using decays to electron pairs [12]. Similar measurements have also been performed by the ATLAS [13] and CMS [14–16] collaborations, although in different kinematic regions.

The measurements of inclusive W and Z boson cross-sections at $\sqrt{s} = 8$ TeV described here are performed following the same procedure as detailed in refs. [8, 9]. The cross-sections are defined for muons with transverse momentum $p_T > 20 \, \text{GeV}/c$ and pseudorapidity in the range $2.0 < \eta < 4.5$. In the case of the Z boson measurements, the invariant mass of the two muons is required to be in the range $60 < M_{\mu\mu} < 120 \, \text{GeV}/c^2$. These kinematic requirements define the fiducial region of the measurement and are referred to as the fiducial requirements in this article. Total cross-sections are presented, as well as differential cross-sections as functions of η of the muons, and of the Z boson rapidity, y_Z, transverse momentum, $p_{T,Z}$, and ϕ_η^* [17]. Here ϕ_η^* is defined as[2]

$$\phi_\eta^* \equiv \frac{\tan{(\phi_{\text{acop}}/2)}}{\cosh{(\Delta\eta/2)}} \,, \tag{1.1}$$

where the angle $\phi_{\text{acop}} = \pi - |\Delta\phi|$ depends on the difference $\Delta\phi$ in azimuthal angle between the two muon momenta, while the difference between their pseudorapidities is denoted by $\Delta\eta$. Differential cross-section ratios and the muon charge asymmetry, arising from the W production charge asymmetry, are also determined as a function of the muon pseudorapidity.

This article is organised as follows: section 2 describes the LHCb detector; section 3 details the selection of W and Z boson candidate samples; section 4 defines the W and Z boson cross-sections and summarises the relevant sources of systematic uncertainty, as well as their estimation; section 5 presents the results and section 6 concludes the article. Appendices A and B provide tables of differential cross-sections and correlations between these measurements.

2 Detector and data set

The LHCb detector [18, 19] is a single-arm forward spectrometer covering the pseudorapidity range $2 < \eta < 5$, designed for the study of particles containing b or c quarks. The detector includes a high-precision tracking system consisting of a silicon-strip vertex detector surrounding the pp interaction region, a large-area silicon-strip detector located upstream of a dipole magnet with a bending power of about 4 Tm, and three stations of silicon-strip detectors and straw drift tubes placed downstream of the magnet. The tracking system provides a measurement of momentum, p, of charged particles with

---

[2]The ϕ_η^* definition in this article is equivalent to the definitions in refs. [9, 10, 12].

a relative uncertainty that varies from 0.5% at low momentum to 1.0% at $200\,\text{GeV}/c$. The minimum distance of a track to a primary vertex, the impact parameter (IP), is measured with a resolution of $(15 + 29/p_{\text{T}})\,\mu\text{m}$, where p_{T} is the component of the momentum transverse to the beam, in GeV/c. Different types of charged hadrons are distinguished using information from two ring-imaging Cherenkov detectors. Photons, electrons and hadrons are identified by a calorimeter system consisting of a scintillating-pad detector (SPD), preshower detectors, an electromagnetic calorimeter and a hadronic calorimeter. Muons are identified by a system composed of alternating layers of iron and multiwire proportional chambers. The online event selection is performed by a trigger [20], which consists of a hardware stage, based on information from the calorimeter and muon systems, followed by a software stage, which applies a full event reconstruction. A requirement that prevents events with high occupancy from dominating the processing time of the software trigger is also applied. This is referred to in this article as the global event cut (GEC).

The measurements presented here are based on pp collision data collected at a centre-of-mass energy of $8\,\text{TeV}$, the integrated luminosity amounting to $1978 \pm 23\,\text{pb}^{-1}$. The absolute luminosity scale was measured during dedicated data-taking periods, using both van der Meer scans [21] and beam-gas imaging methods [22]. Both methods give consistent results, which are combined to give the final luminosity estimate with an uncertainty of 1.16% [23].

Several samples of simulated events are produced to estimate contributions from background processes, to verify efficiencies and to correct data for detector-related effects. In the simulation, pp collisions are generated using PYTHIA 8 [24, 25] with a specific LHCb configuration [26]. Decays of hadronic particles are described by EVTGEN [27], in which final-state radiation is generated using PHOTOS [28]. The interaction of the generated particles with the detector, and its response, are implemented using the GEANT4 toolkit [29, 30] as described in ref. [31].

The W boson yields are determined from fits to the data using signal templates produced with the RESBOS [32–34] generator configured with the CT14 [35] PDF set. The RESBOS generator includes an approximate NNLO calculation, plus a next-to-next-to-leading logarithm approximation for the resummation of the soft gluon radiation.

The results of the analysis are compared to theoretical predictions calculated with the FEWZ [36, 37] generator at NNLO for the PDF sets ABM12 [38], CT10 [39], CT14, HERA1.5 [40], MMHT14 [41] and NNPDF3.0 [42]. All calculations are performed with the renormalisation and factorisation scales set to the electroweak boson mass. Scale uncertainties are estimated by varying these scales by factors of two around the boson mass [43]. Total uncertainties correspond to those coming from the PDF and the strong force coupling strength, α_s, both at 68.3% confidence level (CL), added in quadrature with the scale uncertainties.

3 Event yield

Events for this analysis must satisfy the selection criteria detailed in refs. [8, 9]. The trigger requires a single muon with $p_{\text{T}} > 1.5\,\text{GeV}/c$ at the hardware stage, and includes an upper threshold of 600 hits in the SPD to prevent high-particle multiplicity events from

dominating the processing time. A muon with $p_T > 10\,\mathrm{GeV}/c$ is required at the software stage. In the offline analysis, particles are required to be well-reconstructed, to be identified as muons, and also to pass the fiducial requirements.

Additional selection criteria are applied to the W boson candidates to reduce the contributions of various sources of background. Muons from decays of W bosons are generally isolated from other particles. To define a degree of isolation, a cone with radius $R = \sqrt{\Delta\eta^2 + \Delta\phi^2} = 0.5$ is constructed around the direction of the muon track. Excluding the candidate muon momentum, requiring that there are small amounts of transverse momentum ($p_T^{\mathrm{cone}} < 2\,\mathrm{GeV}/c$) and transverse energy ($E_T^{\mathrm{cone}} < 2\,\mathrm{GeV}$) in the cone reduces background originating from generic QCD events. Requiring the transverse momentum of all other muons in the event to be less than $2\,\mathrm{GeV}/c$ reduces the contamination from $Z \to \mu^+\mu^-$ events. An upper limit on the IP of $40\,\mu\mathrm{m}$ removes candidates in which the muon is not consistent with originating from the primary vertex. Such candidates could be due to electroweak boson decays to tau leptons, which in turn decay to muons, or semileptonic decays of heavy flavour hadrons. Genuine muons are expected to leave low-energy deposits in the electromagnetic and hadronic calorimeters. An upper limit of 4% on the amount of energy that is deposited in the calorimeters relative to the momentum of the track (E_{calo}/pc) reduces the background from energetic pions and kaons punching through the calorimeters to the muon stations. A total of $1\,733\,327$ $W \to \mu\nu$ candidates are identified.

The $W^\pm$ sample purity ($\rho^{W^\pm}$), defined as the ratio of signal to candidate event yield, is determined with a template fit to the positively and negatively charged muon p_T distributions in eight bins of muon pseudorapidity using the method of extended maximum likelihood. Only muons with p_T smaller than $70\,\mathrm{GeV}/c$ are considered. The $W^\pm$ boson signal and the $Z \to \mu^+\mu^-$ background templates are based on distributions predicted by the RESBOS generator. The $Z \to \tau^+\tau^-$ and $W \to \tau\nu$ templates are taken from PYTHIA 8 simulation. The overall fraction of the electroweak background ($Z \to \mu^+\mu^-$, $Z \to \tau^+\tau^-$ and $W \to \tau\nu$ decays) in the W boson candidate sample is determined using a data-driven method to be $(10.84 \pm 0.21)\%$. A template for backgrounds due to misidentified hadrons is taken from data using a sample of randomly triggered pions and kaons that are weighted by their probability to be misidentified as muons. This component is left free to vary in the fit, and is determined to account for about 9.6% of the total candidates. Finally, a template of heavy-flavour decays is obtained from data using muons with an IP of more than $100\,\mu\mathrm{m}$. The fraction of this background is determined from a fit to the muon IP distribution and is found to be $(1.31 \pm 0.09)\%$ of the W boson candidate sample. The momentum calibration for high-p_T muons is performed using the data-driven technique outlined in ref. [44]. A more detailed description of the fit implementation is given in ref. [8]. The fit result in the full η^μ range is presented in figure 1 (left), where the normalised residuals show an imperfect description of the data by the adopted templates, similar to the 7 TeV analysis. The effect of this discrepancy on the signal yield is at the few per mille level. The overall purities are $\rho^{W^+} = (78.91 \pm 0.15)\%$ and $\rho^{W^-} = (77.49 \pm 0.18)\%$.

The invariant mass distribution of dimuon pairs passing the Z candidate requirements is shown in figure 1 (right). In total, $136\,702$ $Z \to \mu^+\mu^-$ candidates are selected. The back-
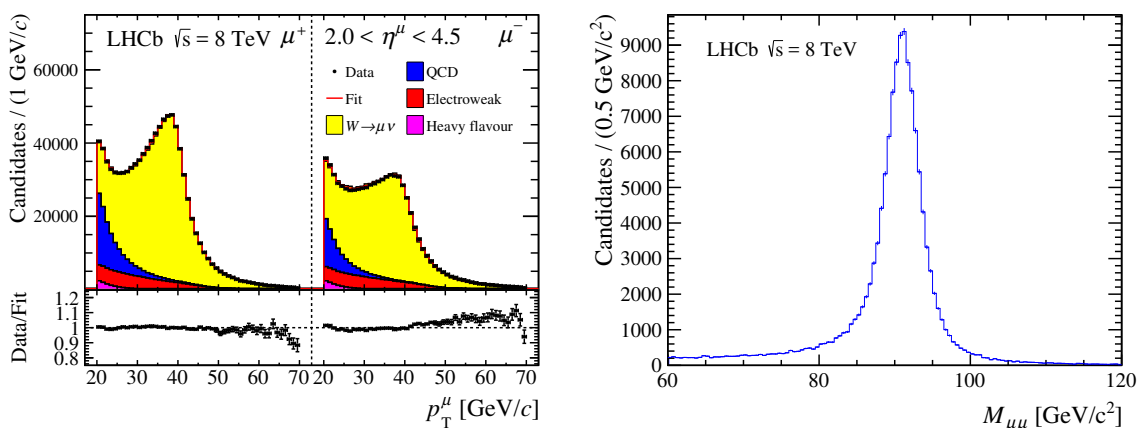
Figure 1. (left) Template fit to the (left panel) positive and (right panel) negative muon p_T spectra in the full η^μ range for W candidates. Data are compared to fitted contributions from $W \to \mu\nu$ signal and QCD, electroweak and heavy flavour backgrounds. (right) Invariant mass distribution of dimuon pairs in the Z candidate sample.

ground contamination is low. Five background sources are considered: decays of heavy flavour hadrons, hadron misidentification, $Z \to \tau^+\tau^-$ decays, $t\bar{t}$ and WW production. The largest sources of background are due to decays of heavy flavour hadrons and hadron misidentification. These backgrounds are determined from data using the techniques discussed in ref. [9]. The heavy-flavour background is estimated from a subset of the candidate sample by placing additional requirements on muon isolation and dimuon vertex quality. The background due to hadron misidentification is estimated using pairs of hadrons from randomly triggered data. These are weighted by the momentum-dependent probabilities for hadrons to be misidentified as muons. The other backgrounds are determined using simulation and the purity is measured to be $\rho^Z = (99.3 \pm 0.2)\%$.

4 Cross-section measurement

Cross-sections are determined in the specified kinematic ranges and are corrected for quantum electrodynamic (QED) final-state radiation (FSR) in order to compare measurements of electroweak boson production in different decay modes and to provide a consistent comparison with next-to-leading order and NNLO QCD predictions. No corrections are applied for initial-state radiation or for electroweak effects and their interplay with QED effects.

The W boson cross-sections are measured as a function of η^μ using the equation

$$\sigma_{W^\pm \to \mu^\pm \nu}(i) = \frac{\rho^{W^\pm}(i)}{\mathcal{L}} \cdot \frac{f_{\text{FSR}}^{W^\pm}(i)}{\varepsilon_{\text{GEC}}(i)} \cdot \frac{N^{W^\pm}(i)}{\varepsilon^{W^\pm}(i)\, \varepsilon_{\text{sel}}^{W^\pm}(i)\, \mathcal{A}^{W^\pm}(i)}, \tag{4.1}$$

where all quantities except for the integrated luminosity, $\mathcal{L}$, are determined in each bin i of η^μ. The number of observed $W^\pm$ boson candidates is denoted by $N^{W^\pm}(i)$. The correction factors for QED final-state radiation are given by $f_{\text{FSR}}^{W^\pm}$ and the efficiency of the requirement on the number of SPD hits in the hardware trigger is represented by ε_{GEC}. The total muon

reconstruction efficiency is denoted by $\varepsilon^{W^\pm}$ while the efficiency of the selection criteria is given by $\varepsilon^{W^\pm}_{\mathrm{sel}}$. The acceptance correction, $\mathcal{A}^{W^\pm}$, accounts for the $70\,\mathrm{GeV}/c$ experimental upper bound in the fit to the muon p_T.

The Z boson cross-sections are measured in bins of y_Z, $p_{\mathrm{T},Z}$, ϕ^*_η and η^μ, by integrating over all but one of these variables. To account for bin migration effects, the cross-section in bin i is determined from the number of events in all bins j with an unfolding matrix U, as follows

$$\sigma_{Z\to\mu^+\mu^-}(i) = \frac{\rho^Z}{\mathcal{L}} \cdot \frac{f^Z_{\mathrm{FSR}}(i)}{\varepsilon_{\mathrm{GEC}}(i)} \cdot \sum_j U(i,j) \left(\sum_k \frac{1}{\varepsilon^Z(\eta_k^{\mu^+}, \eta_k^{\mu^-})} \right)_j . \qquad (4.2)$$

In this expression the index k runs over all candidates contributing to bin j and ε^Z is the pseudorapidity-dependent muon-reconstruction efficiency for event k. The matrix U is determined from simulated data, as described in section 4.6. The QED final-state radiation corrections are denoted by f^Z_{FSR}. The components that are common with the W boson cross-sections defined in eq. (4.1) are the luminosity and the individual muon reconstruction efficiencies.

Although the beam energy does not enter in eqs. (4.1) and (4.2), a related uncertainty is assigned to all cross-sections. More details on these individual components are given below.

4.1 Muon reconstruction efficiencies

The data are corrected for inefficiencies associated with track reconstruction, muon identification, and trigger requirements. All efficiencies are determined from data using the techniques detailed in refs. [8, 9], where the track reconstruction, muon identification, and muon trigger efficiencies are obtained using tag-and-probe methods applied to the Z candidates. The tag and the probe tracks are required to satisfy the fiducial requirements. The tag must be identified as a muon and be consistent with triggering the event, while the probe is defined so that it is unbiased with respect to the requirement for which the efficiency is being measured. The efficiency is studied as a function of several variables, which include both the muon momenta and the detector occupancy. In this analysis, reconstruction, identification and trigger efficiencies are applied as a function of the muon pseudorapidity. The efficiency in each bin of η^μ is defined as the fraction of tag-and-probe candidates where the probe satisfies the corresponding track reconstruction, identification or trigger requirement. All efficiencies are observed to be independent of the muon charge.

The tracking efficiency is determined using probe tracks that are reconstructed by combining hits from the muon stations and the large-area silicon-strip detector. The muon identification efficiency is determined using probe tracks that are reconstructed without using the muon system. The single-muon trigger efficiency is determined using reconstructed muons as probes.

4.2 GEC efficiency

The efficiency of the SPD multiplicity limit at 600 hits in the muon trigger is evaluated from data using two independent methods. The first exploits the fact that the SPD multiplicities of single pp interactions involving a Z boson are rarely above the 600 hit threshold.

The expected SPD multiplicity distribution of signal events is constructed by adding the multiplicities of signal events in single pp interactions to the multiplicities of randomly triggered events, as in ref. [45]. The convolution of the distributions extends to values above 600 hits, and the fraction of events that the trigger rejects can be determined. The second method consists of fitting the SPD multiplicity distribution and extrapolating the fit function to determine the fraction of events that are rejected, as in ref. [9]. Both methods give consistent results and $\varepsilon_{\mathrm{GEC}} = (93.00 \pm 0.32)\%$ is used in this analysis as the overall efficiency. This efficiency depends linearly on y_Z and η^μ, with about 2% variation across the full range. This is accounted for by applying a bin-dependent efficiency correction.

4.3 Final-state radiation

The FSR correction is taken to be the mean of the corrections calculated with HERWIG++ [46] and PYTHIA 8. The corrections are tabulated in appendix A and are about 2.5% on average.

4.4 Selection efficiencies

The efficiency of the additional selection requirements for the W boson candidate samples is evaluated using a sample of Z bosons from data, where one of the muons is excluded to mimic a $W \to \mu\nu$ decay [8]. However, this introduces a bias because the p_T distribution of muons from Z bosons is harder than those from W bosons. Simulation is used to correct for this bias and for the fact that the Z boson sample requires two muons in the LHCb acceptance.

4.5 Acceptance

Only muons with p_T smaller than $70\,\mathrm{GeV}/c$ are considered for the extraction of the W boson signal. A kinematic acceptance correction is required in order to measure cross-sections without this restriction on muon p_T. This correction is evaluated using the RESBOS simulated sample.

4.6 Unfolding the detector response

To correct for detector resolution effects, an unfolding is performed (matrix U of eq. (4.2)) using LHCb simulation and the ROOUNFOLD [47] software package. Only the $p_{T,Z}$ and ϕ_η^* distributions are unfolded. Since y_Z and η^μ are well measured, no unfolding is performed. The momentum resolution in the simulation is calibrated to the data. The data are then unfolded using the iterative Bayesian approach proposed in ref. [48]. Other unfolding techniques [49, 50] give similar results. Additionally, all unfolding methods are tested for model dependence using underlying distributions from leading-order PYTHIA 8, leading-order HERWIG++, as well as next-to-leading order POWHEG [51–53] showered with both PYTHIA 8 and HERWIG++ using the POWHEG matching scheme. The corrections are between 0.5–8.0% as a function of $p_{T,Z}$, and between 0.1–7.0% as a function of ϕ_η^*.

Source	Uncertainty [%]		
	$\sigma_{W^+ \to \mu^+ \nu}$	$\sigma_{W^- \to \mu^- \bar{\nu}}$	$\sigma_{Z \to \mu^+ \mu^-}$
Statistical	0.19	0.23	0.27
Purity	0.28	0.21	0.21
Tracking	0.26	0.24	0.48
Identification	0.11	0.11	0.21
Trigger	0.14	0.13	0.05
GEC	0.40	0.41	0.34
Selection	0.24	0.24	—
Acceptance and FSR	0.16	0.14	0.13
Systematic	0.65	0.61	0.67
Beam energy	1.00	0.86	1.15
Luminosity	1.16	1.16	1.16
Total	1.67	1.59	1.79

Table 1. Summary of the relative uncertainties on the W^+, W^- and Z boson cross-sections.

4.7 Systematic uncertainties

Sources of systematic uncertainty and their effects on the total cross-section measurements from the $\sqrt{s} = 8 \, \text{TeV}$ data set are summarised in table 1. The uncertainty due to the momentum correction is negligible. Uncertainties from external input, e.g. the beam energy and luminosity determinations, are quoted separately from the other contributions.

For the W boson samples, the systematic uncertainty on the purity is estimated by considering different shapes and normalisations of the templates, refitting, and summing in quadrature the largest observed deviation in the results corresponding to each source [8]. The uncertainty on the RESBOS signal template shape includes the effects of the PDF, the factorisation scale and the renormalisation scale. An alternative definition for the QCD background template, potential mismodelling of the lepton p_{T} shape in PYTHIA for events that contain jets, and the normalisations of the background templates are accounted for with additional uncertainties. The total uncertainties on the W^+ and W^- integrated cross-sections from the sample purity are 0.28% and 0.21%. For the Z boson sample, the systematic uncertainty on the purity is determined by considering alternative definitions of the heavy-flavour background samples, and by varying by their uncertainties the probabilities for hadrons to be misidentified as muons. In addition, an uncertainty accounting for the assumption that the purity is the same for all variables and bins of the analysis is evaluated by comparing to cross-section measurements using a binned purity, rather than a global one. The uncertainties on the differential cross-section measurements due to variations in purity are typically less than 1%.

The systematic uncertainty associated with the trigger, identification and tracking efficiencies is determined by re-evaluating all cross-sections with the values of the individual efficiencies increased or decreased by one standard deviation. The full covariance matrix of the differential cross-section measurements is evaluated in this way for each source of

uncertainty. The covariance matrices for each source are added and the diagonal elements of the result determine the total systematic uncertainty due to reconstruction efficiencies. The total uncertainties on the W^+, W^- and Z boson integrated cross-sections due to reconstruction efficiencies are 0.32%, 0.29% and 0.53%.

The GEC efficiency for events containing a Z boson is $\varepsilon_{\mathrm{GEC}}^Z = (93.00 \pm 0.32)\%$. Differences between this efficiency and those for events containing a W^+ or W^- boson are expected to be small, and are thus accounted for with additional systematic uncertainties, as explained in ref. [9]. The values used for the measurements of W boson cross-sections are $\varepsilon_{\mathrm{GEC}}^{W^+} = (93.00 \pm 0.37)\%$ and $\varepsilon_{\mathrm{GEC}}^{W^-} = (93.00 \pm 0.38)\%$.

The uncertainties due to W boson selection efficiencies result in uncertainties on the W^+ and W^- integrated cross-sections of 0.24% and 0.23%. These include the uncertainties that arise due to the difference in W and Z boson muon p_{T} spectra and the correction that accounts for the fact that two muons are required to be inside the LHCb acceptance in the Z boson data sample.

As an estimate of the uncertainty due to the acceptance correction, half the difference between the corrections evaluated using the RESBOS generators and PYTHIA 8 is taken. This results in uncertainties on the W^+ and W^- integrated cross-sections of 0.06% and 0.09%.

The systematic uncertainty on the FSR correction is the quadratic sum of two components. The first is due to the statistical precision of the PYTHIA 8 and HERWIG++ estimates and the second is half of the difference between their central values, where the latter dominates.

The measurements are specified at a pp centre-of-mass energy of $\sqrt{s} = 8$ TeV. The beam energy, and consequently the centre-of-mass energy, is known to 0.65% [54]. The sensitivity of the cross-section to the centre-of-mass energy is studied with the DYNNLO [55] generator at NNLO. Cross-sections are calculated at 1 TeV intervals in centre-of-mass energy and a functional form for the cross-section is determined from a spline interpolation. A 0.65% uncertainty on the centre-of-mass energy induces relative uncertainties of 1.00%, 0.86% and 1.15% on the expected W^+, W^- and Z cross-sections.

The uncertainty on the luminosity determination is 1.16% [23], which represents the largest contribution to the total uncertainty.

5 Results

5.1 Cross-sections at $\sqrt{s} = 8$ TeV

The measured cross-section as a function of muon pseudorapidity in W boson decays is shown in figure 2 (top). Good agreement with the predictions of the FEWZ generator, with six different PDF sets, is observed. Similar conclusions can be drawn from the comparisons of Z boson cross-section measurements with predictions as a function of rapidity, as shown in figure 2 (bottom). All differential cross-sections are detailed in tables 4, 5, 6, 7 and 8 of appendix A.
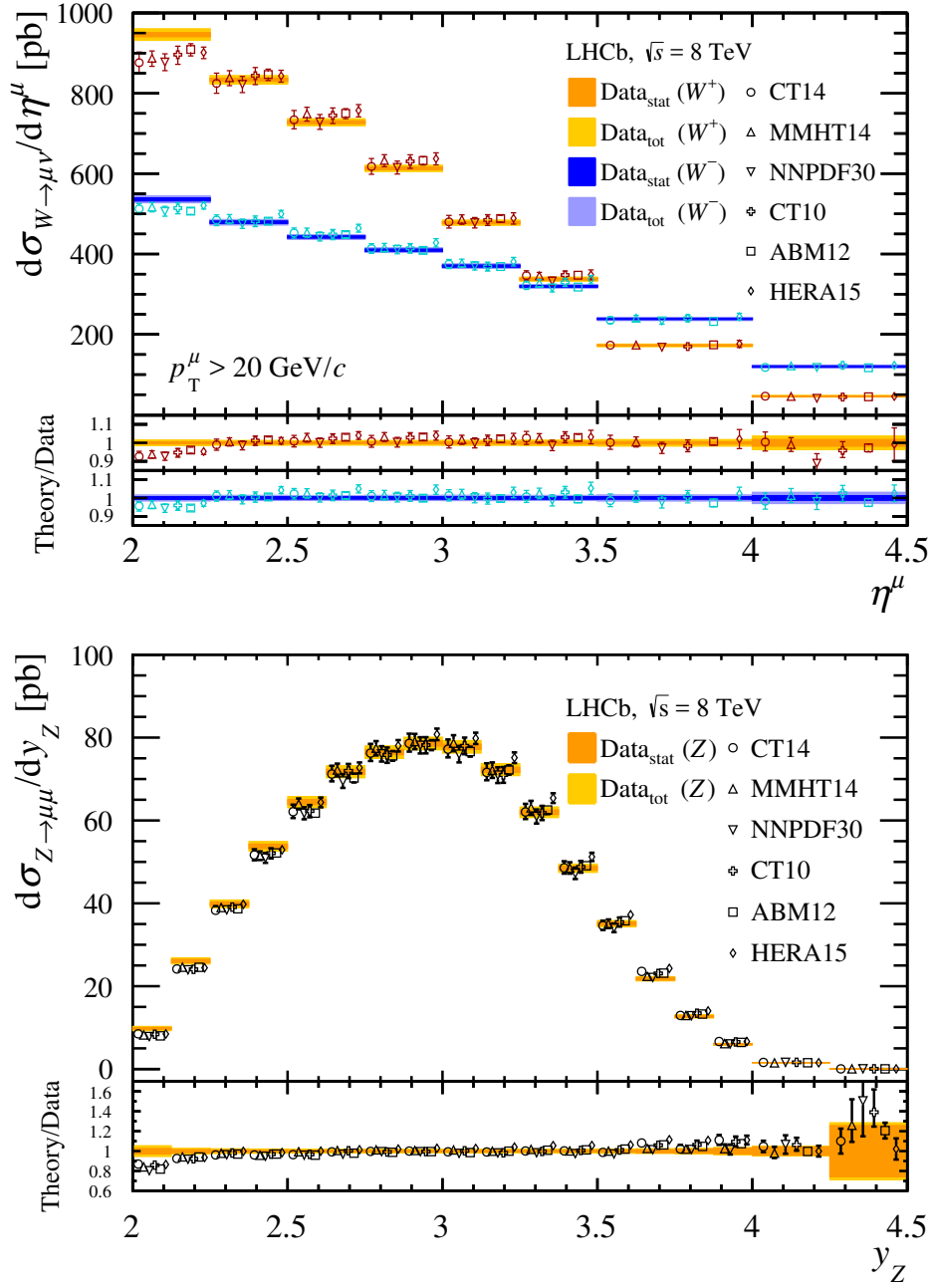
Figure 2. (top) Differential W^+ and W^- boson production cross-section in bins of muon pseudorapidity. (bottom) Differential Z boson production cross-section in bins of boson rapidity. Measurements, represented as bands, are compared to (markers, displaced horizontally for presentation) NNLO predictions with different parameterisations of the PDFs.
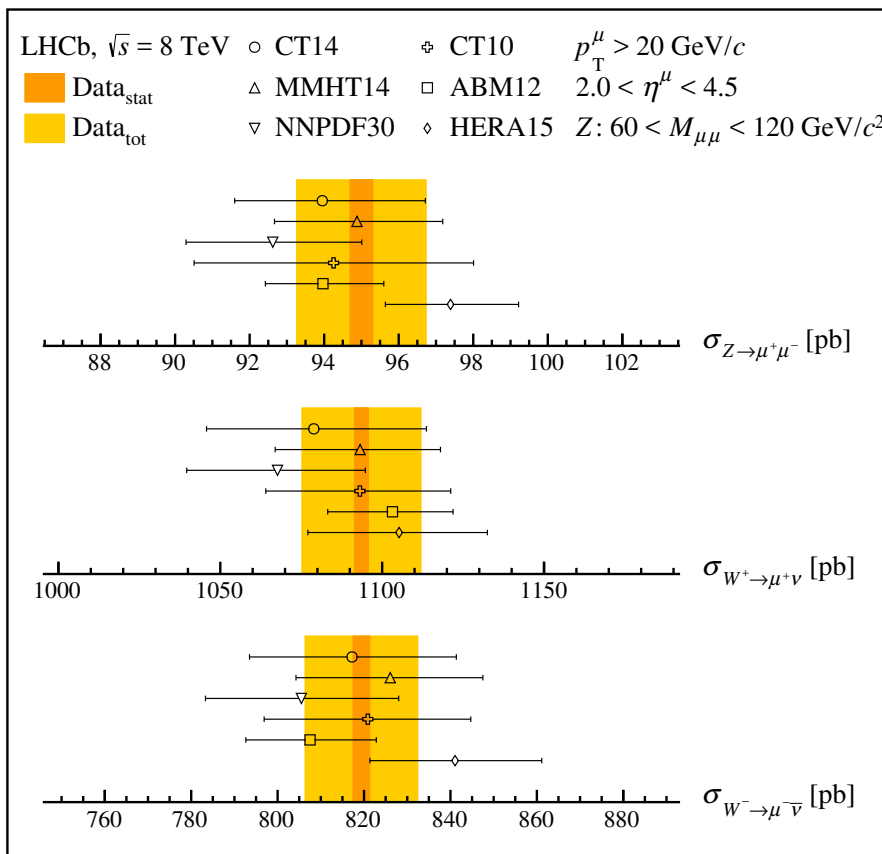
Figure 3. Summary of the W and Z cross-sections. Measurements, represented as bands, are compared to (markers) NNLO predictions with different parameterisations of the PDFs.

The total cross-sections are measured to be

$$\sigma_{W^+\to\mu^+\nu} = 1093.6 \pm 2.1 \pm 7.2 \pm 10.9 \pm 12.7\,\text{pb}\,,$$
$$\sigma_{W^-\to\mu^-\bar{\nu}} = 818.4 \pm 1.9 \pm 5.0 \pm 7.0 \pm 9.5\,\text{pb}\,,$$
$$\sigma_{Z\to\mu^+\mu^-} = 95.0 \pm 0.3 \pm 0.7 \pm 1.1 \pm 1.1\,\text{pb}\,,$$

where the first uncertainties are statistical, the second are systematic, the third are due to the knowledge of the LHC beam energy and the fourth are due to the luminosity measurement. The agreement of the measurements with NNLO predictions given by the FEWZ generator configured with various PDF sets is illustrated in figure 3. Two-dimensional plots of electroweak boson cross-sections are shown in figure 4, where the ellipses correspond to 68.3% CL coverage.

A best linear unbiased estimator [56] is used to combine the Z boson production cross-section at $\sqrt{s} = 8\,\text{TeV}$ measured with the muon and the electron [12] channels. The combined result is

$$\sigma_{Z\to\ell^+\ell^-} = 94.9 \pm 0.2 \pm 0.6 \pm 1.1 \pm 1.1\,\text{pb}\,.$$

Uncertainties due to the GEC, the LHC beam energy and the luminosity measurement are assumed to be fully correlated, while the other uncertainties are assumed to be uncorrelated.
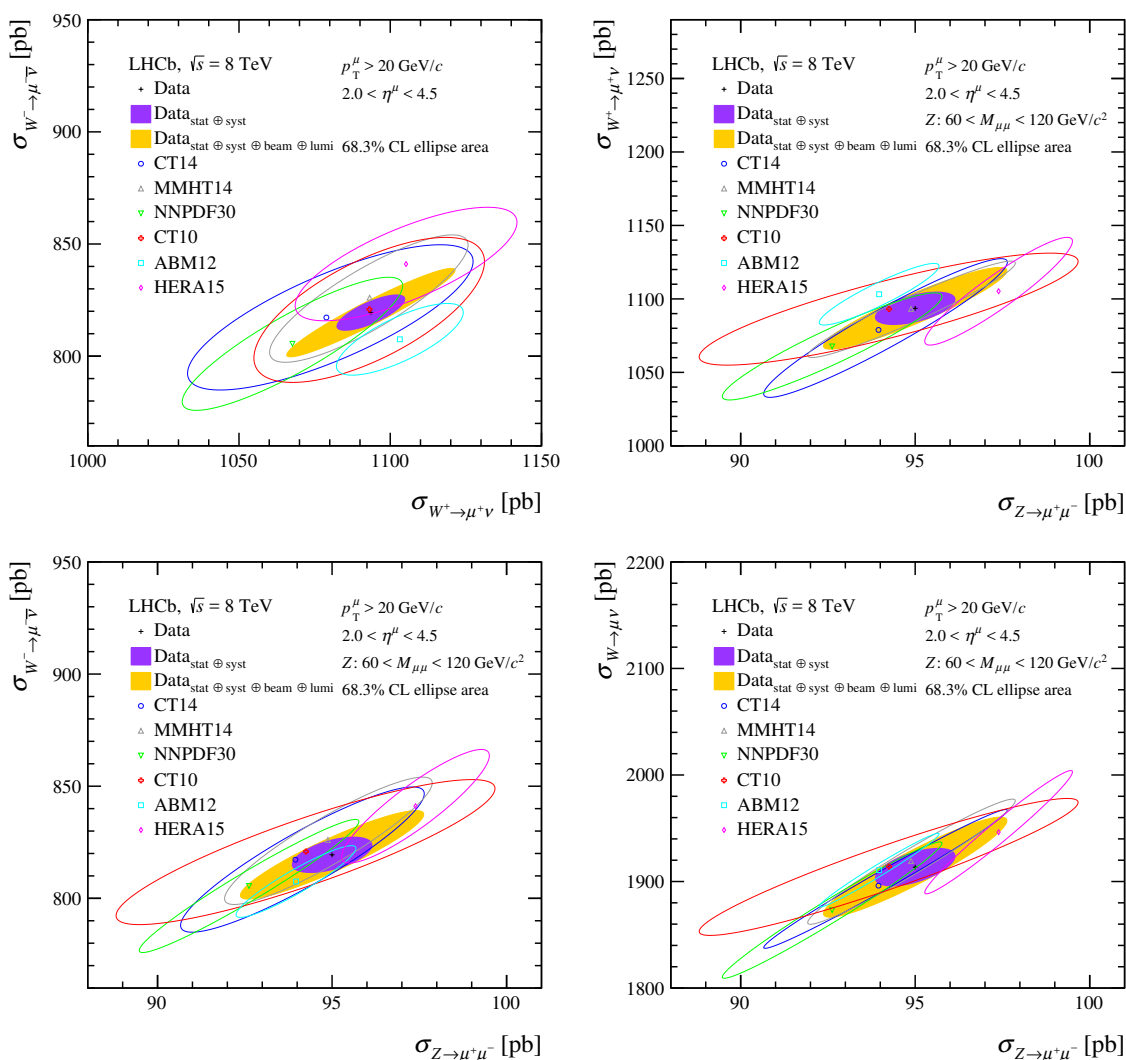
Figure 4. Two-dimensional plots of electroweak boson cross-sections compared to NNLO predictions for various parameterisations of the PDFs. The uncertainties on the theoretical predictions correspond to the PDF uncertainty only. All ellipses correspond to uncertainties at 68.3% CL.

5.2 Ratios of cross-sections at $\sqrt{s} = 8$ TeV

The ratios of electroweak boson production cross-sections are defined as

$$R_{W^\pm} = \frac{\sigma_{W^+ \to \mu^+ \nu}}{\sigma_{W^- \to \mu^- \overline{\nu}}} \,, \tag{5.1}$$

$$R_{W^+ Z} = \frac{\sigma_{W^+ \to \mu^+ \nu}}{\sigma_{Z \to \mu^+ \mu^-}} \,, \tag{5.2}$$

$$R_{W^- Z} = \frac{\sigma_{W^- \to \mu^- \overline{\nu}}}{\sigma_{Z \to \mu^+ \mu^-}} \,, \tag{5.3}$$

$$R_{WZ} = \frac{\sigma_{W^+ \to \mu^+ \nu} + \sigma_{W^- \to \mu^- \overline{\nu}}}{\sigma_{Z \to \mu^+ \mu^-}} \,, \tag{5.4}$$

Source	Uncertainty [%]			
	$R_{W^\pm}$	R_{W^+Z}	R_{W^-Z}	R_{WZ}
Statistical	0.30	0.33	0.36	0.31
Purity	0.25	0.35	0.30	0.30
Tracking	0.05	0.22	0.24	0.23
Identification	0.01	0.11	0.11	0.11
Trigger	0.04	0.10	0.09	0.09
GEC	0.13	0.22	0.23	0.21
Selection	0.10	0.24	0.24	0.23
Acceptance and FSR	0.21	0.21	0.19	0.17
Systematic	0.37	0.59	0.56	0.54
Beam energy	0.14	0.15	0.29	0.21
Total	0.50	0.69	0.73	0.66

Table 2. Summary of the relative uncertainties on the $R_{W^\pm}$, R_{W^+Z}, R_{W^-Z} and R_{WZ} cross-section ratios.

and the muon charge asymmetry as a function of the muon pseudorapidity is defined as

$$A_\mu(\eta_i) = \frac{\sigma_{W^+ \to \mu^+ \nu}(\eta_i) - \sigma_{W^- \to \mu^- \bar{\nu}}(\eta_i)}{\sigma_{W^+ \to \mu^+ \nu}(\eta_i) + \sigma_{W^- \to \mu^- \bar{\nu}}(\eta_i)}. \tag{5.5}$$

The sources of uncertainties contributing to the determination of the ratios are summarised in table 2. With respect to the systematic uncertainties on the cross-sections, many sources cancel or are reduced. The luminosity uncertainty completely cancels in the ratios, as do the correlated components of the GEC efficiency uncertainty. The trigger used to select both samples is identical and most of the uncertainty on the determination of the trigger efficiency cancels. The uncertainties on the tracking and muon identification efficiencies partially cancel in the ratios of W and Z boson cross-sections, as do the uncertainties due to the proton beam energies. The uncertainties on the purities of the W and Z boson selections are uncorrelated and the FSR uncertainties are taken to be uncorrelated. The dominant uncertainties on the ratios are due to the purity and the size of the samples. The correlation coefficients used in the uncertainty calculations are given in tables 15–21 of appendix B.

The W boson cross-section ratio is measured as

$$R_{W^\pm} = 1.336 \pm 0.004 \pm 0.005 \pm 0.002,$$

where the first uncertainty is statistical, the second is systematic and the third is due to the knowledge of the LHC beam energy. The W to Z boson production ratios are found to be

$$R_{W^+Z} = 11.51 \pm 0.04 \pm 0.07 \pm 0.02,$$
$$R_{W^-Z} = 8.62 \pm 0.03 \pm 0.05 \pm 0.02,$$
$$R_{WZ} = 20.13 \pm 0.06 \pm 0.11 \pm 0.04.$$

These measurements, as well as their predictions, are displayed in figure 5. The data are well described by all PDF sets. The W^+ to W^- boson ratio, the charged W to Z boson ratios, and the muon charge asymmetry are determined differentially as a function of muon η, and displayed in figures 6 and 7. Good agreement between measured and predicted values is observed. All differential results are listed in tables 9, 10 and 11 of appendix A.

5.3 Ratios of cross-sections at different centre-of-mass energies

The cross-section measurements detailed in the previous sections were also performed using $1.0\,\mathrm{fb}^{-1}$ of data at 7 TeV [9]. The two sets of measurements are used to make measurements of ratios of quantities at different centre-of-mass energies. The ratios of cross-sections are defined as

$$R_{W^+}^{8/7} = \frac{\sigma_{W^+\to\mu^+\nu}^{8\,\mathrm{TeV}}}{\sigma_{W^+\to\mu^+\nu}^{7\,\mathrm{TeV}}}\,, \tag{5.6}$$

$$R_{W^-}^{8/7} = \frac{\sigma_{W^-\to\mu^-\bar{\nu}}^{8\,\mathrm{TeV}}}{\sigma_{W^-\to\mu^-\bar{\nu}}^{7\,\mathrm{TeV}}}\,, \tag{5.7}$$

$$R_Z^{8/7} = \frac{\sigma_{Z\to\mu^+\mu^-}^{8\,\mathrm{TeV}}}{\sigma_{Z\to\mu^+\mu^-}^{7\,\mathrm{TeV}}}\,, \tag{5.8}$$

and the double ratios of cross-sections are defined as

$$R_{R_{W^\pm}}^{8/7} = \frac{\sigma_{W^+\to\mu^+\nu}^{8\,\mathrm{TeV}}}{\sigma_{W^+\to\mu^+\nu}^{7\,\mathrm{TeV}}}\frac{\sigma_{W^-\to\mu^-\bar{\nu}}^{7\,\mathrm{TeV}}}{\sigma_{W^-\to\mu^-\bar{\nu}}^{8\,\mathrm{TeV}}}\,, \tag{5.9}$$

$$R_{R_{W^+Z}}^{8/7} = \frac{\sigma_{W^+\to\mu^+\nu}^{8\,\mathrm{TeV}}}{\sigma_{W^+\to\mu^+\nu}^{7\,\mathrm{TeV}}}\frac{\sigma_{Z\to\mu^+\mu^-}^{7\,\mathrm{TeV}}}{\sigma_{Z\to\mu^+\mu^-}^{8\,\mathrm{TeV}}}\,, \tag{5.10}$$

$$R_{R_{W^-Z}}^{8/7} = \frac{\sigma_{W^-\to\mu^-\bar{\nu}}^{8\,\mathrm{TeV}}}{\sigma_{W^-\to\mu^-\bar{\nu}}^{7\,\mathrm{TeV}}}\frac{\sigma_{Z\to\mu^+\mu^-}^{7\,\mathrm{TeV}}}{\sigma_{Z\to\mu^+\mu^-}^{8\,\mathrm{TeV}}}\,, \tag{5.11}$$

$$R_{R_{WZ}}^{8/7} = \frac{\sigma_{W\to\mu\nu}^{8\,\mathrm{TeV}}}{\sigma_{W\to\mu\nu}^{7\,\mathrm{TeV}}}\frac{\sigma_{Z\to\mu^+\mu^-}^{7\,\mathrm{TeV}}}{\sigma_{Z\to\mu^+\mu^-}^{8\,\mathrm{TeV}}}\,. \tag{5.12}$$

The following assumptions are made in order to estimate uncertainties on these ratios.

- The uncertainties due to statistically independent samples are uncorrelated, e.g. the uncertainties due to the number of candidates in each measured bin, the uncertainties on the muon reconstruction efficiencies that are uncorrelated between η^μ bins, and the uncertainty that arises from corrections for having two muons inside the acceptance when measuring the selection efficiencies of W bosons and the W boson purity.

- The uncertainties reflecting common methods are correlated, e.g. the Z candidate sample purity estimation, the components of the muon reconstruction efficiencies that are correlated between muon η bins, and the uncertainty that arises when measuring selection efficiencies for W bosons and all aspects of the GEC efficiency.

- The uncertainty due to the FSR correction is taken to be correlated in identical measurement bins and uncorrelated between different measurement bins.

Figure 5. Summary of the cross-section ratios. Measurements, represented as bands, are compared to (markers) NNLO predictions with different parameterisations of the PDFs.

- The beam energy has been directly measured for 4 TeV beams with a precision of 0.65%, but not for 3.5 TeV beams [54]. No additional uncertainty is expected to enter the energy measurement of 3.5 TeV beams, so the relative uncertainty is taken to be the same, and fully correlated between data sets with different centre-of-mass energies.

- The uncertainties ($\delta_i^{\sqrt{s}}$) entering the luminosity estimates are given in ref. [23]. The degree of correlation between the luminosity measurements at different centre-of-mass energies is determined by assigning correlation coefficients (c_i) of 0, 1, [0,0.5], [0.5,1] or [0,1], where the last three represent intervals within which the true correlation is expected to lie. Pseudoexperiments are studied using correlation coefficients that are sampled from both uniform and arcsin distributions across these intervals. With this prescription, the total correlation is calculated using

$$c = \frac{\sum_i c_i \, \delta_i^{8\,\mathrm{TeV}} \delta_i^{7\,\mathrm{TeV}}}{\delta^{8\,\mathrm{TeV}} \delta^{7\,\mathrm{TeV}}} \tag{5.13}$$

and estimated to be 0.55 ± 0.06. A correlation coefficient of 0.55 is used.

A summary of the uncertainties on ratios of quantities at different centre-of-mass energies is given in table 3.
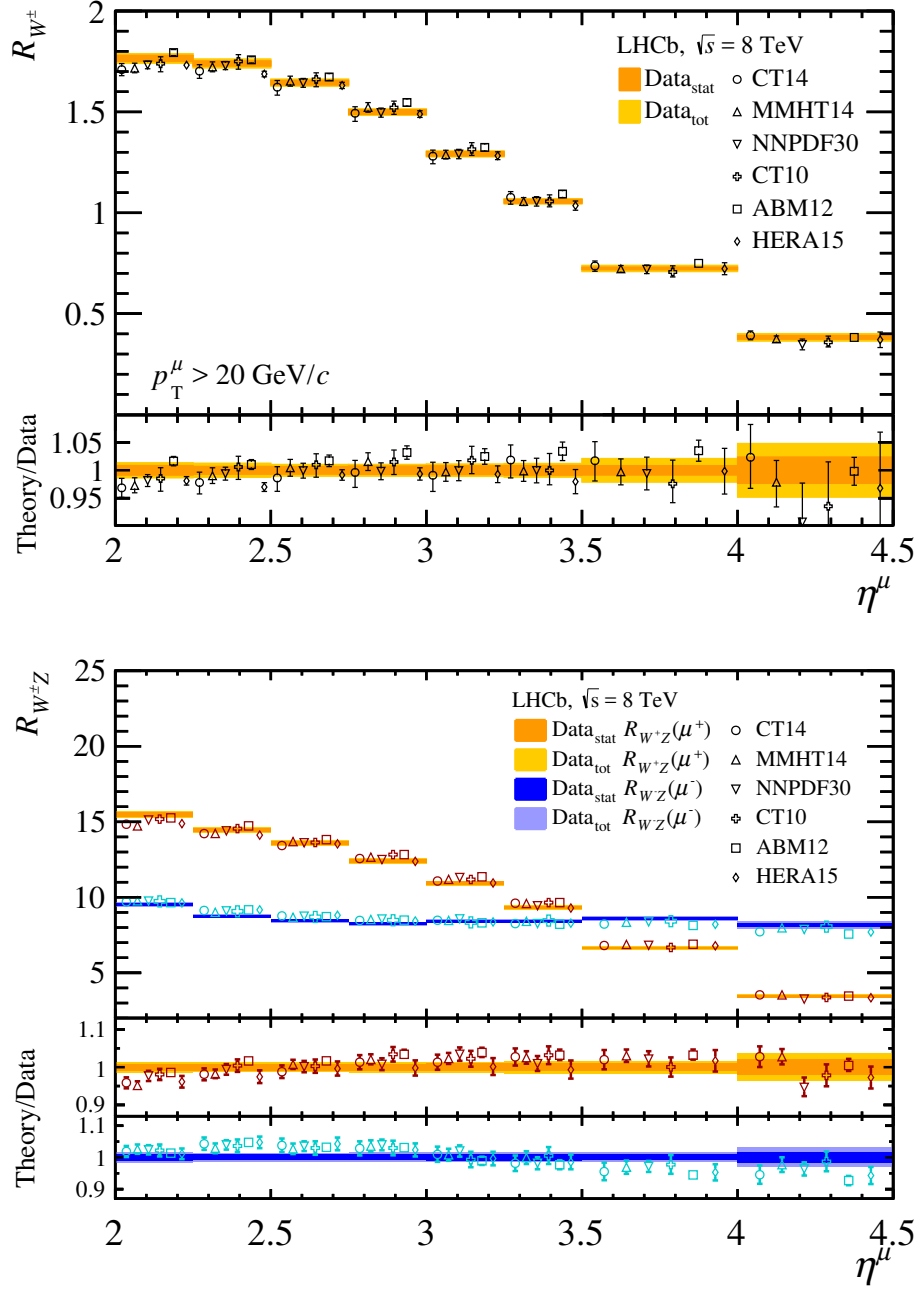
Figure 6. (top) W^+ to W^- cross-section ratio in bins of muon pseudorapidity. (bottom) W^+ (W^-) to Z cross-section ratio in bins of μ^+ (μ^-) pseudorapidity. Measurements, represented as bands, are compared to (markers, displaced horizontally for presentation) NNLO predictions with different parameterisations of the PDFs.
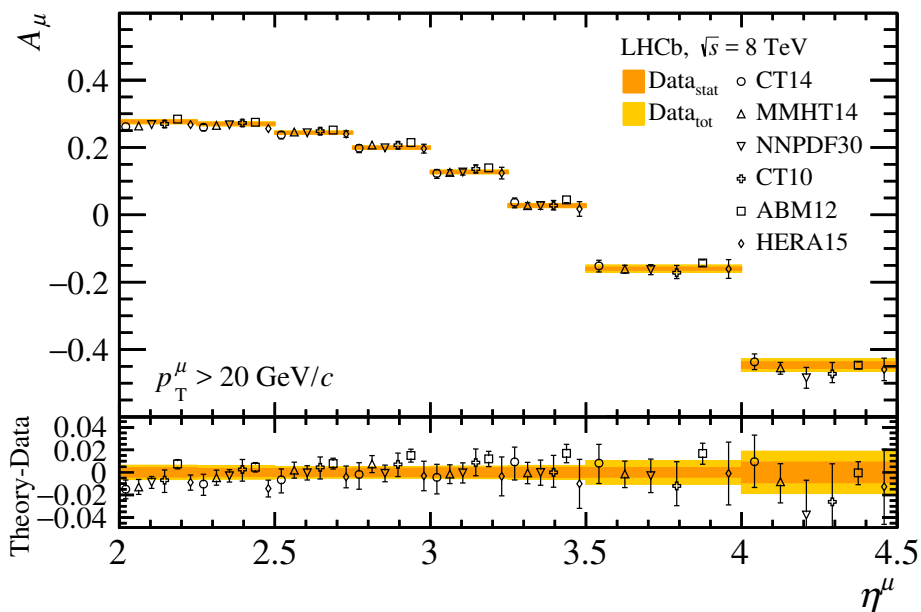
Figure 7. W production charge asymmetry in bins of muon pseudorapidity. Measurements, represented as bands, are compared to (markers, displaced horizontally for presentation) NNLO predictions with different parameterisations of the PDFs.

Source	Uncertainty [%]						
	$R^{8/7}_{W^+}$	$R^{8/7}_{W^-}$	$R^{8/7}_{Z}$	$R^{8/7}_{R_{W^\pm}}$	$R^{8/7}_{R_{W^+ Z}}$	$R^{8/7}_{R_{W^- Z}}$	$R^{8/7}_{R_{WZ}}$
Statistical	0.30	0.37	0.49	0.48	0.58	0.62	0.55
Purity	0.41	0.45	—	0.65	0.41	0.45	0.29
Tracking	0.33	0.27	0.53	0.09	0.23	0.26	0.24
Identification	0.07	0.07	0.13	0.03	0.07	0.06	0.07
Trigger	0.27	0.25	0.09	0.08	0.19	0.16	0.17
GEC	0.15	0.14	0.09	0.07	0.09	0.09	0.08
Selection	0.17	0.17	—	0.04	0.17	0.17	0.16
Acceptance and FSR	0.05	0.06	0.04	0.08	0.07	0.07	0.06
Systematic	0.64	0.63	0.56	0.66	0.55	0.59	0.46
Beam energy	0.06	0.05	0.10	—	0.04	0.05	0.05
Luminosity	1.45	1.45	1.45	—	—	—	—
Total	1.61	1.62	1.63	0.82	0.80	0.86	0.72

Table 3. Summary of the relative uncertainties on the electroweak boson cross-section ratios at different centre-of-mass energies.
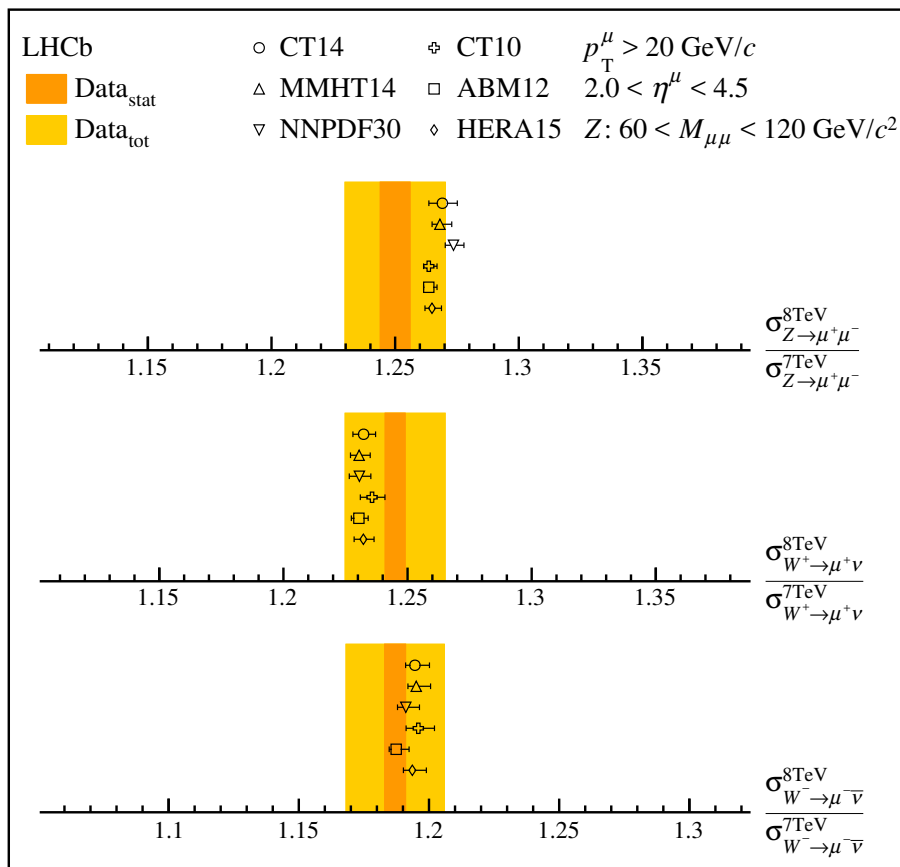
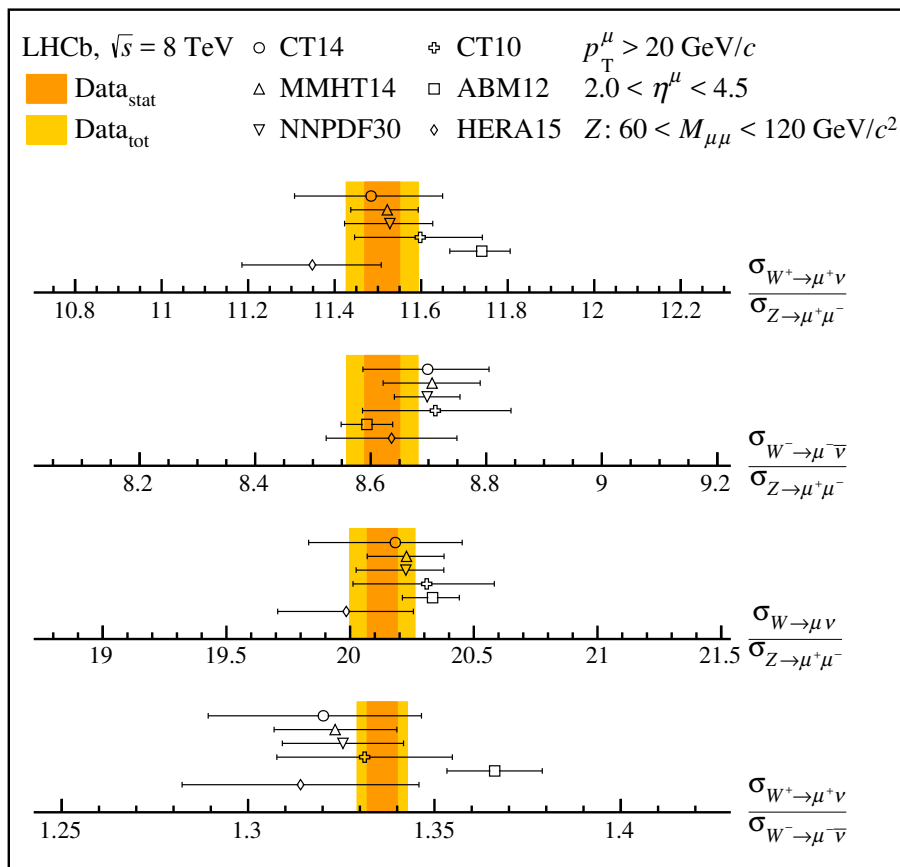**Figure 8.** Summary of the W and Z cross-section ratios at different centre-of-mass energies. Measurements, represented as bands, are compared to (markers) NNLO predictions with different parameterisations of the PDFs.

The cross-section ratios at different centre-of-mass energies, measured for the same kinematic range as the total cross-sections, are

$$R_{W^+}^{8/7} = 1.245 \pm 0.004 \pm 0.008 \pm 0.001 \pm 0.018 \,,$$
$$R_{W^-}^{8/7} = 1.187 \pm 0.004 \pm 0.007 \pm 0.001 \pm 0.017 \,,$$
$$R_Z^{8/7} = 1.250 \pm 0.006 \pm 0.007 \pm 0.001 \pm 0.018 \,,$$

where the first uncertainties are statistical, the second are systematic, the third are due to the knowledge of the LHC beam energy and the fourth are due to the luminosity measurement. The measurements and predictions are in agreement, as shown in figure 8. Compared to figure 3, the variation in the predictions is small. This indicates that the uncertainty due to the PDF is very much reduced, which is also reflected in the calculated uncertainties on the individual PDF predictions.

Even more precise tests can be obtained through the following double ratios of cross-sections, which are independent of the luminosities of either data set. These double ratios
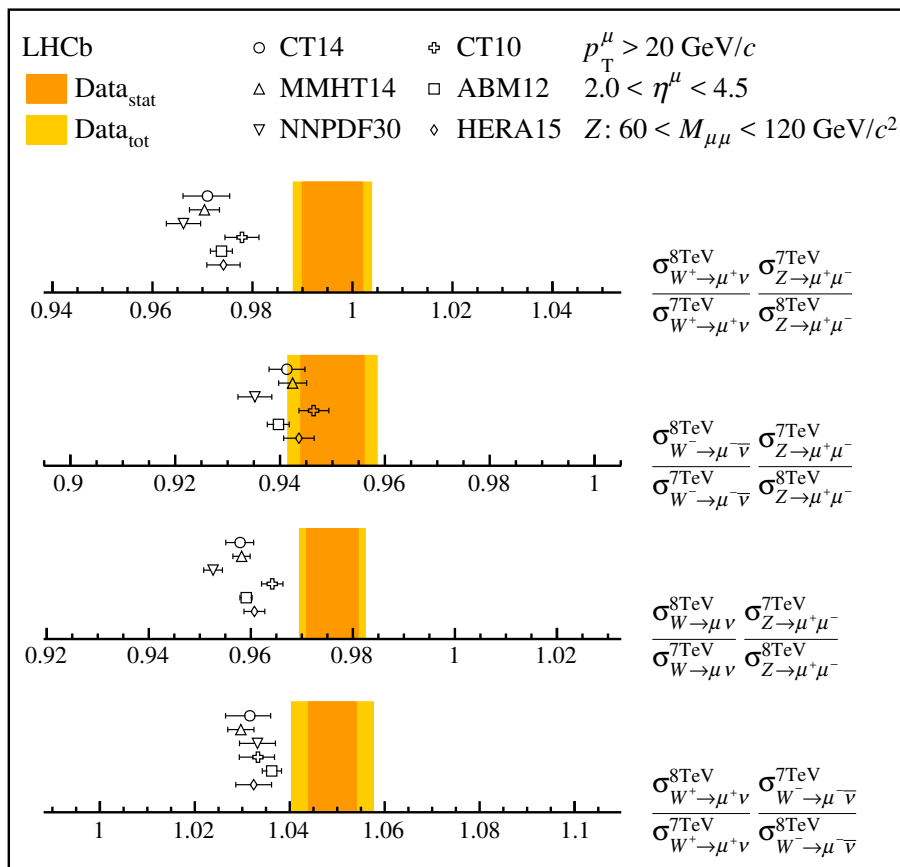
Figure 9. Summary of the cross-section double ratios at different centre-of-mass energies. Measurements, represented as bands, are compared to (markers) NNLO predictions with different parameterisations of the PDFs.

are defined and measured as

$$R^{8/7}_{R_{W^\pm}} = 1.049 \pm 0.005 \pm 0.007\,,$$

$$R^{8/7}_{R_{W^+Z}} = 0.996 \pm 0.006 \pm 0.005\,,$$

$$R^{8/7}_{R_{W^-Z}} = 0.950 \pm 0.006 \pm 0.006\,,$$

$$R^{8/7}_{R_{WZ}} = 0.976 \pm 0.005 \pm 0.004\,,$$

where the first uncertainties are statistical and the second are systematic. The largest source of systematic uncertainty on these ratios is due to the evaluation of the purity of the W boson sample, which ranges between 0.3% and 0.7%. The double ratios are shown in figure 9, where the uncertainties on the predictions due to the PDF, scale, α_s and numerical integration are of similar magnitude. Taking the uncertainty on the SM prediction to be reflected by the spread of the PDF predictions, the maximal deviation between the measured results and the theory is at the level of about 2 standard deviations.

The ratios $R^{8/7}_{R_{W^+Z}}$, $R^{8/7}_{R_{W^-Z}}$ are also measured differentially as a function of muon η. These measurements are displayed in figure 10, where only uncertainties due to PDFs
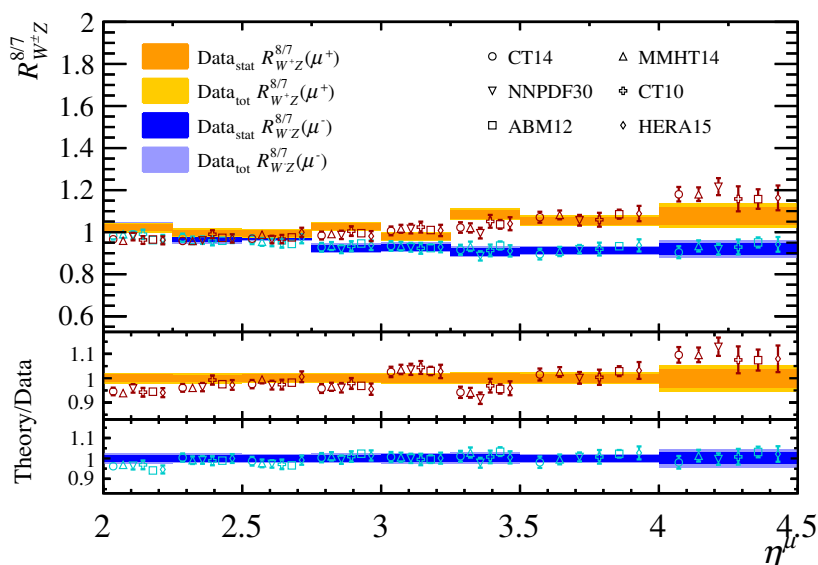
Figure 10. Double ratios of cross-sections at different centre-of-mass energies as a function of muon pseudorapidity. Measurements, represented as bands, are compared to (markers, displaced horizontally for presentation) NNLO predictions with different parameterisations of the PDFs.

are included on the predictions. Good agreement between measurement and prediction is observed, especially for the $R^{8/7}_{R_{W^-Z}}$ ratio. The $R^{8/7}_{R_{W^+Z}}$ ratio increases as a function of η^μ, while the $R^{8/7}_{R_{W^-Z}}$ ratio decreases as a function of η^μ. The PDF uncertainties are largest for the $R^{8/7}_{R_{W^+Z}}$ ratio at high pseudorapidity, suggesting that these measurements can improve the determination of the PDFs in this region. Differential measurements are reported in table 12 of appendix A, along with new differential measurements that were not published in ref. [9] that are required for this analysis (tables 13 and 14).

6   Conclusions

Measurements of forward electroweak boson production at $\sqrt{s} = 8\,\text{TeV}$ are presented and found to be in agreement with NNLO calculations in perturbative quantum chromodynamics. The large degree of correlation between the uncertainties allows for sub-percent determination of the cross-section ratios. These represent the most precise determinations to date of electroweak boson production at the LHC. Using previous results from the $\sqrt{s} = 7\,\text{TeV}$ data set, the evolution with the centre-of-mass energy is studied. Good agreement between measured and predicted cross-section ratios is observed. The experimental uncertainties are dominated by luminosity uncertainties of about 1.5%. Double ratios of cross-sections at different centre-of-mass energies are independent of the luminosity and are thus a more precise class of observables, determined with precision of between 0.7% and 0.9%. In the cross-section ratios, the predictions deviate slightly from the measurements. Such deviations can be expected in BSM extensions that feature new sources of W and Z production. This motivates the extension of this analysis to higher energies, as will be possible with future data.

Acknowledgments

A   Differential measurements

Differential production cross-section measurements as functions of the pseudorapidities of the muons from the decay of the Z boson were not included in the previous publication that describes the analysis of the $\sqrt{s} = 7\,\text{TeV}$ data set [9]. They are provided in this appendix in table 13, along with the related measurements of the differential W to Z boson cross-section ratios in table 14.

η^μ	$\sigma_{W^+ \to \mu^+ \nu}\,[\text{pb}\,]$	$f_{\text{FSR}}^{W^+}$
$2.00 - 2.25$	$236.5 \pm 1.2 \pm 3.2 \pm 2.4 \pm 2.7$	1.0188 ± 0.0047
$2.25 - 2.50$	$208.4 \pm 0.9 \pm 2.2 \pm 2.1 \pm 2.4$	1.0163 ± 0.0028
$2.50 - 2.75$	$182.0 \pm 0.8 \pm 1.8 \pm 1.8 \pm 2.1$	1.0158 ± 0.0025
$2.75 - 3.00$	$153.3 \pm 0.7 \pm 1.6 \pm 1.5 \pm 1.8$	1.0148 ± 0.0028
$3.00 - 3.25$	$119.5 \pm 0.6 \pm 1.3 \pm 1.2 \pm 1.4$	1.0152 ± 0.0032
$3.25 - 3.50$	$84.4 \pm 0.5 \pm 1.0 \pm 0.8 \pm 1.0$	1.0150 ± 0.0046
$3.50 - 4.00$	$86.4 \pm 0.5 \pm 1.2 \pm 0.9 \pm 1.0$	1.0175 ± 0.0045
$4.00 - 4.50$	$23.0 \pm 0.4 \pm 0.7 \pm 0.2 \pm 0.3$	1.0211 ± 0.0087

η^μ	$\sigma_{W^- \to \mu^- \bar{\nu}}\,[\text{pb}\,]$	$f_{\text{FSR}}^{W^-}$
$2.00 - 2.25$	$134.0 \pm 0.9 \pm 1.8 \pm 1.2 \pm 1.6$	1.0172 ± 0.0026
$2.25 - 2.50$	$119.8 \pm 0.7 \pm 1.4 \pm 1.0 \pm 1.4$	1.0155 ± 0.0027
$2.50 - 2.75$	$110.6 \pm 0.6 \pm 1.2 \pm 1.0 \pm 1.3$	1.0153 ± 0.0028
$2.75 - 3.00$	$102.4 \pm 0.6 \pm 1.2 \pm 0.9 \pm 1.2$	1.0162 ± 0.0030
$3.00 - 3.25$	$92.5 \pm 0.6 \pm 1.1 \pm 0.8 \pm 1.1$	1.0160 ± 0.0031
$3.25 - 3.50$	$79.9 \pm 0.5 \pm 0.9 \pm 0.7 \pm 0.9$	1.0176 ± 0.0033
$3.50 - 4.00$	$119.3 \pm 0.6 \pm 1.5 \pm 1.0 \pm 1.4$	1.0200 ± 0.0033
$4.00 - 4.50$	$60.0 \pm 0.7 \pm 1.6 \pm 0.5 \pm 0.7$	1.0243 ± 0.0053

Table 4. Cross-section for (top) W^+ and (bottom) W^- boson production in bins of muon pseudo-rapidity. The first uncertainties are statistical, the second are systematic, the third are due to the knowledge of the LHC beam energy and the fourth are due to the luminosity measurement. The last column lists the final-state radiation correction.

y_Z	$\sigma_{Z \to \mu^+\mu^-}$ [pb]	f^Z_{FSR}
$2.000 - 2.125$	$1.223 \pm 0.033 \pm 0.055 \pm 0.014 \pm 0.014$	1.0466 ± 0.0395
$2.125 - 2.250$	$3.263 \pm 0.051 \pm 0.060 \pm 0.038 \pm 0.038$	1.0305 ± 0.0119
$2.250 - 2.375$	$4.983 \pm 0.062 \pm 0.064 \pm 0.057 \pm 0.058$	1.0277 ± 0.0069
$2.375 - 2.500$	$6.719 \pm 0.070 \pm 0.072 \pm 0.077 \pm 0.078$	1.0252 ± 0.0061
$2.500 - 2.625$	$8.051 \pm 0.076 \pm 0.074 \pm 0.093 \pm 0.094$	1.0264 ± 0.0048
$2.625 - 2.750$	$8.967 \pm 0.079 \pm 0.074 \pm 0.103 \pm 0.105$	1.0257 ± 0.0032
$2.750 - 2.875$	$9.561 \pm 0.081 \pm 0.076 \pm 0.110 \pm 0.112$	1.0258 ± 0.0038
$2.875 - 3.000$	$9.822 \pm 0.082 \pm 0.071 \pm 0.113 \pm 0.115$	1.0252 ± 0.0027
$3.000 - 3.125$	$9.721 \pm 0.081 \pm 0.074 \pm 0.112 \pm 0.114$	1.0282 ± 0.0035
$3.125 - 3.250$	$9.030 \pm 0.078 \pm 0.071 \pm 0.104 \pm 0.105$	1.0264 ± 0.0030
$3.250 - 3.375$	$7.748 \pm 0.072 \pm 0.074 \pm 0.089 \pm 0.090$	1.0261 ± 0.0066
$3.375 - 3.500$	$6.059 \pm 0.063 \pm 0.051 \pm 0.070 \pm 0.071$	1.0248 ± 0.0040
$3.500 - 3.625$	$4.385 \pm 0.054 \pm 0.041 \pm 0.050 \pm 0.051$	1.0258 ± 0.0060
$3.625 - 3.750$	$2.724 \pm 0.042 \pm 0.027 \pm 0.031 \pm 0.032$	1.0228 ± 0.0053
$3.750 - 3.875$	$1.584 \pm 0.032 \pm 0.020 \pm 0.018 \pm 0.019$	1.0180 ± 0.0079
$3.875 - 4.000$	$0.749 \pm 0.022 \pm 0.012 \pm 0.009 \pm 0.009$	1.0207 ± 0.0100
$4.000 - 4.250$	$0.383 \pm 0.016 \pm 0.008 \pm 0.004 \pm 0.004$	1.0183 ± 0.0140
$4.250 - 4.500$	$0.011 \pm 0.003 \pm 0.001 \pm 0.000 \pm 0.000$	1.0177 ± 0.0761

Table 5. Cross-section for Z boson production in bins of boson rapidity. The first uncertainties are statistical, the second are systematic, the third are due to the knowledge of the LHC beam energy and the fourth are due to the luminosity measurement. The last column lists the final-state radiation correction.

$p_{\mathrm{T},Z}\,[\,\mathrm{GeV}/c\,]$	$\sigma_{Z\to\mu^+\mu^-}\,[\,\mathrm{pb}\,]$	f^Z_{FSR}
0.0 – 2.2	$7.903 \pm 0.082 \pm 0.130 \pm 0.091 \pm 0.092$	1.0962 ± 0.0045
2.2 – 3.4	$7.705 \pm 0.080 \pm 0.108 \pm 0.089 \pm 0.090$	1.0788 ± 0.0055
3.4 – 4.6	$7.609 \pm 0.078 \pm 0.080 \pm 0.088 \pm 0.089$	1.0620 ± 0.0039
4.6 – 5.8	$7.073 \pm 0.075 \pm 0.078 \pm 0.081 \pm 0.083$	1.0472 ± 0.0035
5.8 – 7.2	$7.379 \pm 0.078 \pm 0.069 \pm 0.085 \pm 0.086$	1.0290 ± 0.0044
7.2 – 8.7	$6.813 \pm 0.076 \pm 0.074 \pm 0.078 \pm 0.080$	1.0165 ± 0.0060
8.7 – 10.5	$6.751 \pm 0.075 \pm 0.064 \pm 0.078 \pm 0.079$	1.0044 ± 0.0037
10.5 – 12.8	$7.204 \pm 0.078 \pm 0.073 \pm 0.083 \pm 0.084$	0.9953 ± 0.0060
12.8 – 15.4	$6.270 \pm 0.073 \pm 0.053 \pm 0.072 \pm 0.073$	0.9852 ± 0.0035
15.4 – 19.0	$6.534 \pm 0.072 \pm 0.064 \pm 0.075 \pm 0.076$	0.9830 ± 0.0042
19.0 – 24.5	$6.953 \pm 0.071 \pm 0.066 \pm 0.080 \pm 0.081$	0.9853 ± 0.0044
24.5 – 34.0	$6.999 \pm 0.069 \pm 0.062 \pm 0.080 \pm 0.082$	1.0109 ± 0.0031
34.0 – 63.0	$7.602 \pm 0.070 \pm 0.072 \pm 0.087 \pm 0.089$	1.0380 ± 0.0034
63.0 – 270.0	$2.176 \pm 0.037 \pm 0.025 \pm 0.025 \pm 0.025$	1.0604 ± 0.0059

Table 6. Cross-section for Z boson production in bins of boson transverse momentum. The first uncertainties are statistical, the second are systematic, the third are due to the knowledge of the LHC beam energy and the fourth are due to the luminosity measurement. The last column lists the final-state radiation correction.

ϕ^*_η	$\sigma_{Z\to\mu^+\mu^-}\,[\,\mathrm{pb}\,]$	f^Z_{FSR}
0.00 – 0.01	$10.442 \pm 0.077 \pm 0.118 \pm 0.120 \pm 0.122$	1.0367 ± 0.0028
0.01 – 0.02	$9.704 \pm 0.076 \pm 0.116 \pm 0.112 \pm 0.113$	1.0346 ± 0.0031
0.02 – 0.03	$8.510 \pm 0.071 \pm 0.130 \pm 0.098 \pm 0.099$	1.0323 ± 0.0031
0.03 – 0.05	$13.749 \pm 0.089 \pm 0.151 \pm 0.158 \pm 0.161$	1.0288 ± 0.0024
0.05 – 0.07	$10.085 \pm 0.076 \pm 0.119 \pm 0.116 \pm 0.118$	1.0254 ± 0.0036
0.07 – 0.10	$10.662 \pm 0.077 \pm 0.159 \pm 0.123 \pm 0.125$	1.0211 ± 0.0030
0.10 – 0.15	$10.575 \pm 0.077 \pm 0.133 \pm 0.122 \pm 0.123$	1.0196 ± 0.0029
0.15 – 0.20	$6.322 \pm 0.059 \pm 0.074 \pm 0.073 \pm 0.074$	1.0177 ± 0.0034
0.20 – 0.30	$6.681 \pm 0.061 \pm 0.085 \pm 0.077 \pm 0.078$	1.0188 ± 0.0039
0.30 – 0.40	$3.213 \pm 0.042 \pm 0.064 \pm 0.037 \pm 0.038$	1.0210 ± 0.0064
0.40 – 0.60	$2.837 \pm 0.040 \pm 0.055 \pm 0.033 \pm 0.033$	1.0251 ± 0.0065
0.60 – 0.80	$1.030 \pm 0.024 \pm 0.027 \pm 0.012 \pm 0.012$	1.0258 ± 0.0114
0.80 – 1.20	$0.670 \pm 0.020 \pm 0.030 \pm 0.008 \pm 0.008$	1.0269 ± 0.0110
1.20 – 2.00	$0.263 \pm 0.013 \pm 0.022 \pm 0.003 \pm 0.003$	1.0276 ± 0.0210
2.00 – 4.00	$0.094 \pm 0.008 \pm 0.023 \pm 0.001 \pm 0.001$	1.0345 ± 0.0396

Table 7. Cross-section for Z boson production in bins of boson ϕ^*_η. The first uncertainties are statistical, the second are systematic, the third are due to the knowledge of the LHC beam energy and the fourth are due to the luminosity measurement. The last column lists the final-state radiation correction.

η^μ	$\sigma_{Z\to\mu^+\mu^-}(\eta^{\mu^+})$ [pb]	$f_{\rm FSR}^Z$
$2.00 - 2.25$	$15.28 \pm 0.11 \pm 0.18 \pm 0.18 \pm 0.18$	1.0293 ± 0.0036
$2.25 - 2.50$	$14.39 \pm 0.10 \pm 0.13 \pm 0.17 \pm 0.17$	1.0250 ± 0.0027
$2.50 - 2.75$	$13.39 \pm 0.10 \pm 0.11 \pm 0.15 \pm 0.16$	1.0244 ± 0.0044
$2.75 - 3.00$	$12.37 \pm 0.09 \pm 0.10 \pm 0.14 \pm 0.14$	1.0240 ± 0.0033
$3.00 - 3.25$	$10.93 \pm 0.09 \pm 0.09 \pm 0.13 \pm 0.13$	1.0234 ± 0.0037
$3.25 - 3.50$	$9.02 \pm 0.08 \pm 0.08 \pm 0.10 \pm 0.11$	1.0246 ± 0.0046
$3.50 - 4.00$	$12.94 \pm 0.09 \pm 0.10 \pm 0.15 \pm 0.15$	1.0269 ± 0.0033
$4.00 - 4.50$	$6.67 \pm 0.07 \pm 0.07 \pm 0.08 \pm 0.08$	1.0365 ± 0.0038

η^μ	$\sigma_{Z\to\mu^+\mu^-}(\eta^{\mu^-})$ [pb]	$f_{\rm FSR}^Z$
$2.00 - 2.25$	$14.07 \pm 0.10 \pm 0.18 \pm 0.16 \pm 0.16$	1.0291 ± 0.0056
$2.25 - 2.50$	$13.68 \pm 0.10 \pm 0.13 \pm 0.16 \pm 0.16$	1.0254 ± 0.0028
$2.50 - 2.75$	$13.09 \pm 0.10 \pm 0.10 \pm 0.15 \pm 0.15$	1.0251 ± 0.0028
$2.75 - 3.00$	$12.43 \pm 0.09 \pm 0.11 \pm 0.14 \pm 0.15$	1.0239 ± 0.0033
$3.00 - 3.25$	$11.01 \pm 0.09 \pm 0.10 \pm 0.13 \pm 0.13$	1.0227 ± 0.0041
$3.25 - 3.50$	$9.49 \pm 0.08 \pm 0.08 \pm 0.11 \pm 0.11$	1.0246 ± 0.0042
$3.50 - 4.00$	$13.85 \pm 0.10 \pm 0.11 \pm 0.16 \pm 0.16$	1.0268 ± 0.0036
$4.00 - 4.50$	$7.35 \pm 0.07 \pm 0.07 \pm 0.09 \pm 0.09$	1.0353 ± 0.0055

Table 8. Cross-section for Z boson production in bins of muon pseudorapidity. The first uncertainties are statistical, the second are systematic, the third are due to the knowledge of the LHC beam energy and the fourth are due to the luminosity measurement. The last column lists the final-state radiation correction.

η^{μ^+}	R_{W^+Z}
$2.00 - 2.25$	$15.478 \pm 0.134 \pm 0.174 \pm 0.024 \pm 0.001$
$2.25 - 2.50$	$14.490 \pm 0.119 \pm 0.136 \pm 0.022 \pm 0.001$
$2.50 - 2.75$	$13.593 \pm 0.112 \pm 0.137 \pm 0.020 \pm 0.001$
$2.75 - 3.00$	$12.406 \pm 0.108 \pm 0.126 \pm 0.019 \pm 0.001$
$3.00 - 3.25$	$10.937 \pm 0.102 \pm 0.115 \pm 0.016 \pm 0.001$
$3.25 - 3.50$	$9.353 \pm 0.097 \pm 0.114 \pm 0.015 \pm 0.001$
$3.50 - 4.00$	$6.677 \pm 0.063 \pm 0.093 \pm 0.010 \pm 0.001$
$4.00 - 4.50$	$3.444 \pm 0.072 \pm 0.103 \pm 0.005 \pm 0.000$

η^{μ^-}	R_{W^-Z}
$2.00 - 2.25$	$9.521 \pm 0.095 \pm 0.117 \pm 0.028 \pm 0.001$
$2.25 - 2.50$	$8.754 \pm 0.080 \pm 0.090 \pm 0.025 \pm 0.001$
$2.50 - 2.75$	$8.449 \pm 0.076 \pm 0.086 \pm 0.025 \pm 0.001$
$2.75 - 3.00$	$8.235 \pm 0.077 \pm 0.089 \pm 0.024 \pm 0.000$
$3.00 - 3.25$	$8.400 \pm 0.082 \pm 0.096 \pm 0.024 \pm 0.001$
$3.25 - 3.50$	$8.414 \pm 0.088 \pm 0.096 \pm 0.024 \pm 0.000$
$3.50 - 4.00$	$8.615 \pm 0.075 \pm 0.107 \pm 0.025 \pm 0.001$
$4.00 - 4.50$	$8.166 \pm 0.130 \pm 0.215 \pm 0.023 \pm 0.000$

Table 9. (Top) W^+ and (bottom) W^- to Z cross-section ratios in bins of muon pseudorapidity. The first uncertainties are statistical, the second are systematic, the third are due to the knowledge of the LHC beam energy and the fourth are due to the luminosity measurement.

η^{μ}	$R_{W^\pm}$
$2.00 - 2.25$	$1.765 \pm 0.015 \pm 0.018 \pm 0.003$
$2.25 - 2.50$	$1.740 \pm 0.012 \pm 0.018 \pm 0.002$
$2.50 - 2.75$	$1.645 \pm 0.011 \pm 0.013 \pm 0.002$
$2.75 - 3.00$	$1.499 \pm 0.011 \pm 0.011 \pm 0.002$
$3.00 - 3.25$	$1.292 \pm 0.010 \pm 0.010 \pm 0.002$
$3.25 - 3.50$	$1.057 \pm 0.009 \pm 0.009 \pm 0.002$
$3.50 - 4.00$	$0.724 \pm 0.006 \pm 0.014 \pm 0.001$
$4.00 - 4.50$	$0.383 \pm 0.009 \pm 0.016 \pm 0.001$

Table 10. W^+ to W^- cross-section ratio in bins of muon pseudorapidity. The first uncertainties are statistical, the second are systematic and the third are due to the knowledge of the LHC beam energy.

η^{μ}	A_{μ} (%)
$2.00 - 2.25$	$27.67 \pm 0.39 \pm 0.48 \pm 0.07$
$2.25 - 2.50$	$27.02 \pm 0.33 \pm 0.47 \pm 0.07$
$2.50 - 2.75$	$24.39 \pm 0.32 \pm 0.37 \pm 0.07$
$2.75 - 3.00$	$19.96 \pm 0.35 \pm 0.34 \pm 0.07$
$3.00 - 3.25$	$12.74 \pm 0.38 \pm 0.37 \pm 0.07$
$3.25 - 3.50$	$2.75 \pm 0.43 \pm 0.42 \pm 0.07$
$3.50 - 4.00$	$-15.99 \pm 0.39 \pm 0.96 \pm 0.07$
$4.00 - 4.50$	$-44.63 \pm 0.89 \pm 1.64 \pm 0.06$

Table 11. Lepton charge asymmetry in bins of muon pseudorapidity. The first uncertainties are statistical, the second are systematic and the third are due to the knowledge of the LHC beam energy.

$\eta^{\mu^{+}}$	$R^{8/7}_{R_{W^{+}Z}}$
$2.00 - 2.25$	$1.022 \pm 0.015 \pm 0.016$
$2.25 - 2.50$	$0.997 \pm 0.014 \pm 0.016$
$2.50 - 2.75$	$0.993 \pm 0.014 \pm 0.013$
$2.75 - 3.00$	$1.027 \pm 0.016 \pm 0.013$
$3.00 - 3.25$	$0.981 \pm 0.017 \pm 0.014$
$3.25 - 3.50$	$1.085 \pm 0.020 \pm 0.017$
$3.50 - 4.00$	$1.055 \pm 0.018 \pm 0.016$
$4.00 - 4.50$	$1.077 \pm 0.041 \pm 0.043$

$\eta^{\mu^{-}}$	$R^{8/7}_{R_{W^{-}Z}}$
$2.00 - 2.25$	$1.022 \pm 0.017 \pm 0.018$
$2.25 - 2.50$	$0.969 \pm 0.015 \pm 0.017$
$2.50 - 2.75$	$0.977 \pm 0.015 \pm 0.013$
$2.75 - 3.00$	$0.925 \pm 0.015 \pm 0.017$
$3.00 - 3.25$	$0.928 \pm 0.016 \pm 0.016$
$3.25 - 3.50$	$0.906 \pm 0.017 \pm 0.020$
$3.50 - 4.00$	$0.912 \pm 0.014 \pm 0.014$
$4.00 - 4.50$	$0.922 \pm 0.026 \pm 0.033$

Table 12. Ratios of (top) W^{+} and (bottom) W^{-} to Z cross-section ratios at different centre-of-mass energies in bins of muon pseudorapidity. The first uncertainty is statistical and the second is systematic.

η^μ	$\sigma_{Z\to\mu^+\mu^-}(\eta^{\mu^+})$ [pb]	f^Z_{FSR}
$2.00 - 2.25$	$12.69 \pm 0.13 \pm 0.16 \pm 0.16 \pm 0.22$	1.0290 ± 0.0038
$2.25 - 2.50$	$12.31 \pm 0.13 \pm 0.13 \pm 0.15 \pm 0.21$	1.0246 ± 0.0031
$2.50 - 2.75$	$11.27 \pm 0.12 \pm 0.10 \pm 0.14 \pm 0.19$	1.0237 ± 0.0040
$2.75 - 3.00$	$10.16 \pm 0.11 \pm 0.10 \pm 0.13 \pm 0.18$	1.0242 ± 0.0044
$3.00 - 3.25$	$8.44 \pm 0.10 \pm 0.08 \pm 0.11 \pm 0.15$	1.0235 ± 0.0033
$3.25 - 3.50$	$7.15 \pm 0.10 \pm 0.07 \pm 0.09 \pm 0.12$	1.0258 ± 0.0045
$3.50 - 4.00$	$9.48 \pm 0.11 \pm 0.08 \pm 0.12 \pm 0.16$	1.0286 ± 0.0032
$4.00 - 4.50$	$4.49 \pm 0.08 \pm 0.05 \pm 0.06 \pm 0.08$	1.0386 ± 0.0044

η^μ	$\sigma_{Z\to\mu^+\mu^-}(\eta^{\mu^-})$ [pb]	f^Z_{FSR}
$2.00 - 2.25$	$11.93 \pm 0.13 \pm 0.19 \pm 0.15 \pm 0.21$	1.0294 ± 0.0047
$2.25 - 2.50$	$11.61 \pm 0.12 \pm 0.14 \pm 0.15 \pm 0.20$	1.0251 ± 0.0026
$2.50 - 2.75$	$11.12 \pm 0.12 \pm 0.12 \pm 0.14 \pm 0.19$	1.0245 ± 0.0030
$2.75 - 3.00$	$9.93 \pm 0.11 \pm 0.10 \pm 0.12 \pm 0.17$	1.0238 ± 0.0031
$3.00 - 3.25$	$8.91 \pm 0.11 \pm 0.11 \pm 0.11 \pm 0.15$	1.0236 ± 0.0044
$3.25 - 3.50$	$7.39 \pm 0.10 \pm 0.08 \pm 0.09 \pm 0.13$	1.0253 ± 0.0048
$3.50 - 4.00$	$10.16 \pm 0.11 \pm 0.11 \pm 0.13 \pm 0.18$	1.0269 ± 0.0047
$4.00 - 4.50$	$4.95 \pm 0.08 \pm 0.09 \pm 0.06 \pm 0.09$	1.0376 ± 0.0055

Table 13. Cross-section for Z boson production in bins of muon pseudorapidity at $\sqrt{s} = 7\,\mathrm{TeV}$. The first uncertainties are statistical, the second are systematic, the third are due to the knowledge of the LHC beam energy and the fourth are due to the luminosity measurement. The last column lists the final-state radiation correction.

η^{μ^+}	R_{W^+Z}
$2.00 - 2.25$	$15.152 \pm 0.182 \pm 0.231 \pm 0.029 \pm 0.001$
$2.25 - 2.50$	$14.529 \pm 0.167 \pm 0.230 \pm 0.028 \pm 0.001$
$2.50 - 2.75$	$13.689 \pm 0.164 \pm 0.176 \pm 0.026 \pm 0.001$
$2.75 - 3.00$	$12.079 \pm 0.153 \pm 0.153 \pm 0.023 \pm 0.001$
$3.00 - 3.25$	$11.176 \pm 0.157 \pm 0.151 \pm 0.021 \pm 0.001$
$3.25 - 3.50$	$8.623 \pm 0.134 \pm 0.132 \pm 0.016 \pm 0.001$
$3.50 - 4.00$	$6.330 \pm 0.091 \pm 0.076 \pm 0.012 \pm 0.001$
$4.00 - 4.50$	$3.198 \pm 0.101 \pm 0.093 \pm 0.006 \pm 0.000$

η^{μ^-}	R_{W^-Z}
$2.00 - 2.25$	$9.314 \pm 0.126 \pm 0.162 \pm 0.032 \pm 0.001$
$2.25 - 2.50$	$9.030 \pm 0.115 \pm 0.151 \pm 0.031 \pm 0.001$
$2.50 - 2.75$	$8.647 \pm 0.112 \pm 0.112 \pm 0.029 \pm 0.001$
$2.75 - 3.00$	$8.907 \pm 0.121 \pm 0.150 \pm 0.030 \pm 0.001$
$3.00 - 3.25$	$9.054 \pm 0.129 \pm 0.156 \pm 0.031 \pm 0.001$
$3.25 - 3.50$	$9.285 \pm 0.143 \pm 0.202 \pm 0.032 \pm 0.001$
$3.50 - 4.00$	$9.443 \pm 0.124 \pm 0.126 \pm 0.032 \pm 0.001$
$4.00 - 4.50$	$8.858 \pm 0.212 \pm 0.243 \pm 0.030 \pm 0.001$

Table 14. (Top) W^+ and (bottom) W^- to Z cross-section ratios in bins of muon pseudorapidity at $\sqrt{s} = 7\,\text{TeV}$. The first uncertainties are statistical, the second are systematic, the third are due to the knowledge of the LHC beam energy and the fourth are due to the luminosity measurement.

B   Correlation matrices

η^μ	2–2.25		2.25–2.5		2.5–2.75		2.75–3		3–3.25		3.25–3.5		3.5–4		4–4.5		
2–2.25	1																W^+
	0.67	1															W^-
2.25–2.5	0.20	0.10	1														W^+
	0.07	0.21	0.54	1													W^-
2.5–2.75	0.13	0.24	0.12	0.23	1												W^+
	0.05	0.18	0.03	0.22	0.64	1											W^-
2.75–3	0.06	0.22	0.03	0.28	0.26	0.27	1										W^+
	0.04	0.21	0.00	0.25	0.25	0.31	0.70	1									W^-
3–3.25	0.07	0.22	0.03	0.28	0.25	0.26	0.33	0.30	1								W^+
	0.06	0.22	0.03	0.28	0.26	0.27	0.32	0.32	0.68	1							W^-
3.25–3.5	0.03	0.23	−0.01	0.28	0.28	0.27	0.35	0.33	0.34	0.32	1						W^+
	0.07	0.23	0.04	0.23	0.30	0.29	0.28	0.32	0.27	0.28	0.63	1					W^-
3.5–4	−0.00	0.26	−0.06	0.33	0.31	0.32	0.41	0.39	0.40	0.38	0.45	0.36	1				W^+
	0.14	−0.06	0.20	−0.04	−0.13	−0.04	−0.08	−0.11	−0.07	−0.07	−0.17	−0.19	−0.04	1			W^-
4–4.5	−0.07	0.14	−0.14	0.24	0.14	0.23	0.32	0.29	0.32	0.26	0.35	0.22	0.45	−0.15	1		W^+
	0.12	−0.09	0.17	−0.11	−0.18	−0.14	−0.17	−0.19	−0.15	−0.18	−0.23	−0.24	−0.31	0.48	0.05	1	W^-
	W^+	W^-	W^+	W^-	W^+	W^-	W^+	W^-	W^+	W^-	W^+	W^-	W^+	W^-	W^+	W^-	

Table 15. Correlation coefficients between the differential W^+ and W^- cross-sections in bins of muon η. The LHC beam energy and luminosity uncertainties, which are fully correlated between cross-section measurements, are excluded.

– 30 –

y_Z	2–2.125	2.125–2.25	2.25–2.375	2.375–2.5	2.5–2.625	2.625–2.75	2.75–2.875	2.875–3	3–3.125	3.125–3.25	3.25–3.375	3.375–3.5	3.5–3.625	3.625–3.75	3.75–3.875	3.875–4	4–4.25	4.25–4.5
2–2.125	1																	
2.125–2.25	0.19	1																
2.25–2.375	0.17	0.27	1															
2.375–2.5	0.16	0.26	0.28	1														
2.5–2.625	0.16	0.25	0.28	0.29	1													
2.625–2.75	0.15	0.24	0.27	0.29	0.30	1												
2.75–2.875	0.14	0.23	0.26	0.28	0.29	0.30	1											
2.875–3	0.14	0.21	0.25	0.27	0.29	0.30	0.30	1										
3–3.125	0.13	0.20	0.23	0.25	0.27	0.28	0.29	0.29	1									
3.125–3.25	0.11	0.17	0.20	0.23	0.25	0.26	0.27	0.28	0.27	1								
3.25–3.375	0.09	0.14	0.16	0.18	0.20	0.22	0.22	0.23	0.23	0.23	1							
3.375–3.5	0.08	0.12	0.15	0.17	0.19	0.20	0.21	0.22	0.22	0.22	0.20	1						
3.5–3.625	0.07	0.10	0.12	0.14	0.16	0.17	0.18	0.19	0.19	0.20	0.18	0.19	1					
3.625–3.75	0.06	0.08	0.10	0.11	0.13	0.14	0.15	0.16	0.16	0.17	0.16	0.16	0.15	1				
3.75–3.875	0.05	0.07	0.08	0.09	0.10	0.11	0.11	0.12	0.13	0.13	0.12	0.13	0.12	0.11	1			
3.875–4	0.03	0.05	0.06	0.06	0.07	0.08	0.08	0.09	0.09	0.10	0.09	0.10	0.09	0.08	0.07	1		
4–4.25	0.03	0.04	0.04	0.05	0.05	0.06	0.06	0.06	0.07	0.07	0.07	0.08	0.07	0.07	0.06	0.05	1	
4.25–4.5	0.01	0.01	0.01	0.01	0.01	0.01	0.01	0.01	0.01	0.01	0.01	0.02	0.02	0.01	0.01	0.01	0.01	1

Table 16. Correlation coefficients between the differential Z cross-section in bins of y_Z. The LHC beam energy and luminosity uncertainties, which are fully correlated between cross-section measurements, are excluded.

$p_{\mathrm{T},Z}$ [GeV/c]	0.0–2.2	2.2–3.4	3.4–4.6	4.6–5.8	5.8–7.2	7.2–8.7	8.7–10.5	10.5–12.8	12.8–15.4	15.4–19	19–24.5	24.5–34	34–63	63–270
0.0–2.2	1													
2.2–3.4	0.06	1												
3.4–4.6	0.08	0.16	1											
4.6–5.8	0.13	0.09	0.20	1										
5.8–7.2	0.15	0.16	0.12	0.19	1									
7.2–8.7	0.14	0.16	0.18	0.11	0.17	1								
8.7–10.5	0.14	0.16	0.20	0.19	0.14	0.15	1							
10.5–12.8	0.14	0.16	0.19	0.19	0.21	0.14	0.12	1						
12.8–15.4	0.15	0.17	0.20	0.19	0.22	0.20	0.17	0.11	1					
15.4–19	0.14	0.16	0.20	0.19	0.21	0.19	0.21	0.18	0.11	1				
19–24.5	0.15	0.17	0.21	0.20	0.22	0.20	0.21	0.21	0.21	0.13	1			
24.5–34	0.16	0.18	0.22	0.21	0.23	0.21	0.22	0.22	0.23	0.22	0.17	1		
34–63	0.16	0.18	0.22	0.21	0.23	0.21	0.22	0.22	0.23	0.22	0.23	0.21	1	
63–270	0.11	0.12	0.15	0.14	0.16	0.15	0.15	0.15	0.16	0.15	0.16	0.17	0.15	1

Table 17. Correlation coefficients between the differential Z cross-section in bins of $p_{\mathrm{T},Z}$. The LHC beam energy and luminosity uncertainties, which are fully correlated between cross-section measurements, are excluded.

ϕ_η^*	0.00–0.01	0.01–0.02	0.02–0.03	0.03–0.05	0.05–0.07	0.07–0.10	0.10–0.15	0.15–0.20	0.20–0.30	0.30–0.40	0.40–0.60	0.60–0.80	0.80–1.20	1.20–2.00	2.00–4.00
0.00–0.01	1														
0.01–0.02	0.50	1													
0.02–0.03	0.42	0.39	1												
0.03–0.05	0.57	0.55	0.44	1											
0.05–0.07	0.52	0.50	0.41	0.55	1										
0.07–0.10	0.44	0.42	0.34	0.47	0.42	1									
0.10–0.15	0.50	0.48	0.40	0.54	0.49	0.41	1								
0.15–0.20	0.49	0.47	0.38	0.52	0.48	0.40	0.46	1							
0.20–0.30	0.47	0.45	0.37	0.50	0.45	0.39	0.44	0.43	1						
0.30–0.40	0.31	0.30	0.24	0.33	0.30	0.26	0.29	0.29	0.27	1					
0.40–0.60	0.31	0.29	0.24	0.33	0.30	0.25	0.29	0.28	0.27	0.18	1				
0.60–0.80	0.21	0.20	0.16	0.23	0.20	0.17	0.20	0.19	0.19	0.12	0.12	1			
0.80–1.20	0.13	0.13	0.10	0.14	0.13	0.11	0.13	0.12	0.12	0.08	0.08	0.05	1		
1.20–2.00	0.07	0.07	0.06	0.08	0.07	0.06	0.07	0.07	0.06	0.04	0.04	0.03	0.02	1	
2.00–4.00	0.02	0.02	0.02	0.02	0.02	0.02	0.02	0.02	0.02	0.01	0.01	0.01	0.01	0.00	1

Table 18. Correlation coefficients between the differential Z cross-section in bins of ϕ_η^*. The LHC beam energy and luminosity uncertainties, which are fully correlated between cross-section measurements, are excluded.

η^μ		y_Z
		2–2.125	2.125–2.25	2.25–2.375	2.375–2.5	2.5–2.625	2.625–2.75	2.75–2.875	2.875–3	3–3.125	3.125–3.25	3.25–3.375	3.375–3.5	3.5–3.625	3.625–3.75	3.75–3.875	3.875–4	4–4.25	4.25–4.5
2–2.25	W^+	0.23	0.30	0.28	0.27	0.26	0.25	0.24	0.23	0.21	0.18	0.15	0.13	0.11	0.10	0.07	0.05	0.04	0.01
	W^-	0.21	0.28	0.26	0.25	0.24	0.24	0.22	0.21	0.20	0.17	0.14	0.12	0.11	0.09	0.07	0.05	0.04	0.01
2.25–2.5	W^+	0.05	0.15	0.21	0.20	0.20	0.20	0.20	0.19	0.18	0.16	0.14	0.12	0.10	0.08	0.06	0.04	0.03	0.01
	W^-	0.04	0.14	0.19	0.18	0.18	0.18	0.18	0.17	0.16	0.15	0.12	0.11	0.09	0.07	0.05	0.04	0.03	0.00
2.5–2.75	W^+	0.04	0.07	0.12	0.15	0.16	0.17	0.17	0.17	0.16	0.15	0.13	0.13	0.11	0.08	0.06	0.05	0.03	0.01
	W^-	0.04	0.07	0.11	0.14	0.15	0.15	0.15	0.15	0.15	0.14	0.12	0.12	0.10	0.08	0.06	0.04	0.03	0.01
2.75–3	W^+	0.05	0.08	0.10	0.13	0.16	0.17	0.17	0.17	0.16	0.16	0.14	0.13	0.12	0.09	0.07	0.05	0.03	0.01
	W^-	0.05	0.07	0.09	0.12	0.14	0.15	0.15	0.16	0.15	0.14	0.12	0.12	0.11	0.08	0.06	0.04	0.03	0.01
3–3.25	W^+	0.06	0.08	0.10	0.11	0.14	0.16	0.15	0.17	0.15	0.16	0.14	0.14	0.12	0.10	0.08	0.05	0.03	0.01
	W^-	0.05	0.08	0.09	0.10	0.13	0.15	0.15	0.16	0.15	0.15	0.13	0.13	0.11	0.09	0.07	0.05	0.03	0.01
3.25–3.5	W^+	0.04	0.06	0.07	0.09	0.10	0.11	0.12	0.13	0.13	0.12	0.11	0.11	0.09	0.08	0.06	0.04	0.03	0.00
	W^-	0.04	0.06	0.08	0.09	0.10	0.12	0.13	0.13	0.13	0.13	0.11	0.11	0.10	0.08	0.06	0.04	0.03	0.00
3.5–4	W^+	0.04	0.06	0.07	0.08	0.09	0.10	0.11	0.12	0.12	0.12	0.11	0.11	0.10	0.09	0.07	0.05	0.04	0.00
	W^-	0.04	0.06	0.08	0.09	0.10	0.11	0.12	0.13	0.14	0.14	0.12	0.12	0.11	0.10	0.08	0.06	0.04	0.01
4–4.5	W^+	0.02	0.03	0.04	0.04	0.04	0.04	0.05	0.05	0.06	0.06	0.06	0.07	0.06	0.06	0.05	0.04	0.04	0.01
	W^-	0.03	0.04	0.04	0.05	0.05	0.06	0.06	0.06	0.07	0.07	0.07	0.08	0.08	0.07	0.06	0.05	0.04	0.01

Table 19. Correlation coefficients between differential W and Z cross-sections in bins of muon η and y_Z, respectively. The LHC beam energy and luminosity uncertainties, which are fully correlated between cross-section measurements, are excluded.

η^{μ^+}	2.00–2.25	2.25–2.50	2.50–2.75	2.75–3.00	3.00–3.25	3.25–3.50	3.50–4.00	4.00–4.50
2.00–2.25	1							
2.25–2.50	0.31	1						
2.50–2.75	0.30	0.27	1					
2.75–3.00	0.31	0.28	0.26	1				
3.00–3.25	0.32	0.28	0.26	0.27	1			
3.25–3.50	0.27	0.25	0.23	0.23	0.23	1		
3.50–4.00	0.33	0.30	0.28	0.28	0.28	0.25	1	
4.00–4.50	0.28	0.25	0.23	0.24	0.23	0.20	0.23	1

η^{μ^-}	2.00–2.25	2.25–2.50	2.50–2.75	2.75–3.00	3.00–3.25	3.25–3.50	3.50–4.00	4.00–4.50
2.00–2.25	1							
2.25–2.50	0.29	1						
2.50–2.75	0.30	0.29	1					
2.75–3.00	0.30	0.28	0.28	1				
3.00–3.25	0.30	0.27	0.27	0.27	1			
3.25–3.50	0.27	0.25	0.25	0.24	0.24	1		
3.50–4.00	0.31	0.29	0.29	0.28	0.28	0.25	1	
4.00–4.50	0.28	0.25	0.25	0.24	0.24	0.21	0.24	1

Table 20. Correlation coefficients between the differential Z cross-sections in bins of (top) η^{μ^+} and (bottom) η^{μ^-}. The LHC beam energy and luminosity uncertainties, which are fully correlated between cross-section measurements, are excluded.

W	η^{μ^+}	Z							
		2.00–2.25	2.25–2.50	2.50–2.75	2.75–3.00	3.00–3.25	3.25–3.50	3.50–4.00	4.00–4.50
	2.00–2.25	0.48	0.19	0.19	0.20	0.20	0.18	0.22	0.18
	2.25–2.50	0.15	0.38	0.16	0.16	0.16	0.14	0.17	0.14
	2.50–2.75	0.14	0.14	0.26	0.14	0.14	0.13	0.16	0.12
	2.75–3.00	0.14	0.14	0.14	0.26	0.15	0.13	0.16	0.12
	3.00–3.25	0.15	0.14	0.14	0.15	0.25	0.13	0.15	0.12
	3.25–3.50	0.11	0.11	0.11	0.11	0.11	0.17	0.12	0.09
	3.50–4.00	0.10	0.10	0.11	0.11	0.11	0.10	0.18	0.08
	4.00–4.50	0.06	0.06	0.06	0.06	0.06	0.05	0.06	0.11

W	η^{μ^-}	Z							
		2.00–2.25	2.25–2.50	2.50–2.75	2.75–3.00	3.00–3.25	3.25–3.50	3.50–4.00	4.00–4.50
	2.00–2.25	0.43	0.18	0.19	0.19	0.19	0.18	0.21	0.18
	2.25–2.50	0.13	0.35	0.15	0.15	0.14	0.14	0.16	0.13
	2.50–2.75	0.12	0.13	0.25	0.13	0.13	0.12	0.14	0.12
	2.75–3.00	0.12	0.13	0.14	0.24	0.13	0.12	0.14	0.12
	3.00–3.25	0.13	0.13	0.14	0.14	0.23	0.13	0.15	0.12
	3.25–3.50	0.11	0.11	0.12	0.12	0.12	0.18	0.12	0.10
	3.50–4.00	0.11	0.12	0.12	0.12	0.12	0.11	0.20	0.10
	4.00–4.50	0.07	0.06	0.07	0.07	0.07	0.06	0.07	0.13

Table 21. Correlation coefficients between the differential W and Z cross-sections in bins of (top) η^{μ^+} and (bottom) η^{μ^-}. The LHC beam energy and luminosity uncertainties, which are fully correlated between cross-section measurements, are excluded.

References

[1] P.J. Rijken and W.L. van Neerven, *Order α_s^2 contributions to the Drell-Yan cross-section at fixed target energies*, *Phys. Rev.* **D 51** (1995) 44 [hep-ph/9408366] [INSPIRE].

[2] R. Hamberg, W.L. van Neerven and T. Matsuura, *A complete calculation of the order α_s^2 correction to the Drell-Yan K factor*, *Nucl. Phys.* **B 359** (1991) 343 [*Erratum ibid.* **B 644** (2002) 403] [INSPIRE].

[3] W.L. van Neerven and E.B. Zijlstra, *The $O(\alpha_s^2)$ corrected Drell-Yan K factor in the DIS and MS scheme*, *Nucl. Phys.* **B 382** (1992) 11 [*Erratum ibid.* **B 680** (2004) 513] [INSPIRE].

[4] R.V. Harlander and W.B. Kilgore, *Next-to-next-to-leading order Higgs production at hadron colliders*, *Phys. Rev. Lett.* **88** (2002) 201801 [hep-ph/0201206] [INSPIRE].

[5] C. Anastasiou, L.J. Dixon, K. Melnikov and F. Petriello, *High precision QCD at hadron colliders: Electroweak gauge boson rapidity distributions at NNLO*, *Phys. Rev.* **D 69** (2004) 094008 [hep-ph/0312266] [INSPIRE].

[6] R.S. Thorne, A.D. Martin, W.J. Stirling and G. Watt, *Parton Distributions and QCD at LHCb*, arXiv:0808.1847 [INSPIRE].

[7] M.L. Mangano and J. Rojo, *Cross section Ratios between different CM energies at the LHC: opportunities for precision measurements and BSM sensitivity*, *JHEP* **08** (2012) 010 [arXiv:1206.3557] [INSPIRE].

[8] LHCb collaboration, *Measurement of the forward W boson cross-section in pp collisions at $\sqrt{s} = 7\,TeV$*, *JHEP* **12** (2014) 079 [arXiv:1408.4354] [INSPIRE].

[9] LHCb collaboration, *Measurement of the forward Z boson production cross-section in pp collisions at $\sqrt{s} = 7\,TeV$*, *JHEP* **08** (2015) 039 [arXiv:1505.07024] [INSPIRE].

[10] LHCb collaboration, *Measurement of the cross-section for $Z \to e^+e^-$ production in pp collisions at $\sqrt{s} = 7\,TeV$*, *JHEP* **02** (2013) 106 [arXiv:1212.4620] [INSPIRE].

[11] LHCb collaboration, *A study of the Z production cross-section in pp collisions at $\sqrt{s} = 7\,TeV$ using tau final states*, *JHEP* **01** (2013) 111 [arXiv:1210.6289] [INSPIRE].

[12] LHCb collaboration, *Measurement of forward $Z \to e^+e^-$ production at $\sqrt{s} = 8\,TeV$*, *JHEP* **05** (2015) 109 [arXiv:1503.00963] [INSPIRE].

[13] ATLAS collaboration, *Measurement of the inclusive $W^{\pm}$ and Z/γ^* cross sections in the e and μ decay channels in pp collisions at $\sqrt{s} = 7\,TeV$ with the ATLAS detector*, *Phys. Rev.* **D 85** (2012) 072004 [arXiv:1109.5141] [INSPIRE].

[14] CMS collaboration, *Measurement of the Inclusive W and Z Production Cross sections in pp Collisions at $\sqrt{s} = 7\,TeV$*, *JHEP* **10** (2011) 132 [arXiv:1107.4789] [INSPIRE].

[15] CMS collaboration, *Measurement of inclusive W and Z boson production cross sections in pp collisions at $\sqrt{s} = 8\,TeV$*, *Phys. Rev. Lett.* **112** (2014) 191802 [arXiv:1402.0923] [INSPIRE].

[16] CMS collaboration, *Measurement of the Z boson differential cross section in transverse momentum and rapidity in proton-proton collisions at $8\,TeV$*, *Phys. Lett.* **B 749** (2015) 187 [arXiv:1504.03511] [INSPIRE].

[17] A. Banfi, S. Redford, M. Vesterinen, P. Waller and T.R. Wyatt, *Optimisation of variables for studying dilepton transverse momentum distributions at hadron colliders*, *Eur. Phys. J.* **C 71** (2011) 1600 [arXiv:1009.1580] [INSPIRE].

[18] LHCb collaboration, *The LHCb Detector at the LHC*, 2008 *JINST* **3** S08005 [INSPIRE].

[19] LHCb collaboration, *LHCb Detector Performance*, *Int. J. Mod. Phys.* **A 30** (2015) 1530022 [arXiv:1412.6352] [INSPIRE].

[20] R. Aaij et al., *The LHCb Trigger and its Performance in 2011*, 2013 *JINST* **8** P04022 [arXiv:1211.3055] [INSPIRE].

[21] S. van der Meer, *Calibration of the effective beam height in the ISR*, ISR-PO/68-31, (1968).

[22] M. Ferro-Luzzi, *Proposal for an absolute luminosity determination in colliding beam experiments using vertex detection of beam-gas interactions*, *Nucl. Instrum. Meth.* **A 553** (2005) 388 [INSPIRE].

[23] LHCb collaboration, *Precision luminosity measurements at LHCb*, 2014 *JINST* **9** P12005 [arXiv:1410.0149] [INSPIRE].

[24] T. Sjöstrand, S. Mrenna and P.Z. Skands, *A Brief Introduction to PYTHIA 8.1*, *Comput. Phys. Commun.* **178** (2008) 852 [arXiv:0710.3820] [INSPIRE].

[25] T. Sjöstrand, S. Mrenna and P.Z. Skands, *PYTHIA 6.4 Physics and Manual*, *JHEP* **05** (2006) 026 [hep-ph/0603175] [INSPIRE].

[26] LHCb collaboration, *Handling of the generation of primary events in Gauss, the LHCb simulation framework*, *J. Phys. Conf. Ser.* **331** (2011) 032047 [INSPIRE].

[27] D.J. Lange, *The EvtGen particle decay simulation package*, *Nucl. Instrum. Meth.* **A 462** (2001) 152 [INSPIRE].

[28] P. Golonka and Z. Was, *PHOTOS Monte Carlo: A precision tool for QED corrections in Z and W decays*, *Eur. Phys. J.* **C 45** (2006) 97 [hep-ph/0506026] [INSPIRE].

[29] GEANT4 collaboration, J. Allison et al., *Geant4 developments and applications*, *IEEE Trans. Nucl. Sci.* **53** (2006) 270.

[30] GEANT4 collaboration, S. Agostinelli et al., *GEANT4: A simulation toolkit*, *Nucl. Instrum. Meth.* **A 506** (2003) 250 [INSPIRE].

[31] LHCb collaboration, *The LHCb simulation application, Gauss: Design, evolution and experience*, *J. Phys. Conf. Ser.* **331** (2011) 032023 [INSPIRE].

[32] G.A. Ladinsky and C.P. Yuan, *The Nonperturbative regime in QCD resummation for gauge boson production at hadron colliders*, *Phys. Rev.* **D 50** (1994) 4239 [hep-ph/9311341] [INSPIRE].

[33] C. Balázs and C.P. Yuan, *Soft gluon effects on lepton pairs at hadron colliders*, *Phys. Rev.* **D 56** (1997) 5558 [hep-ph/9704258] [INSPIRE].

[34] F. Landry, R. Brock, P.M. Nadolsky and C.P. Yuan, *Tevatron Run-1 Z boson data and Collins-Soper-Sterman resummation formalism*, *Phys. Rev.* **D 67** (2003) 073016 [hep-ph/0212159] [INSPIRE].

[35] S. Dulat et al., *The CT14 Global Analysis of Quantum Chromodynamics*, arXiv:1506.07443 [INSPIRE].

[36] Y. Li and F. Petriello, *Combining QCD and electroweak corrections to dilepton production in FEWZ*, *Phys. Rev.* **D 86** (2012) 094034 [arXiv:1208.5967] [INSPIRE].

[37] R. Gavin, Y. Li, F. Petriello and S. Quackenbush, *FEWZ 2.0: A code for hadronic Z production at next-to-next-to-leading order*, *Comput. Phys. Commun.* **182** (2011) 2388 [arXiv:1011.3540] [INSPIRE].

[38] S. Alekhin, J. Blumlein and S. Moch, *The ABM parton distributions tuned to LHC data*, *Phys. Rev.* **D 89** (2014) 054028 [arXiv:1310.3059] [INSPIRE].

[39] H.-L. Lai et al., *New parton distributions for collider physics*, *Phys. Rev.* **D 82** (2010) 074024 [arXiv:1007.2241] [INSPIRE].

[40] ZEUS, H1 collaborations, F.D. Aaron et al., *Combined Measurement and QCD Analysis of the Inclusive $e^{\pm}p$ Scattering Cross sections at HERA*, *JHEP* **01** (2010) 109 [arXiv:0911.0884] [INSPIRE].

[41] L.A. Harland-Lang, A.D. Martin, P. Motylinski and R.S. Thorne, *Parton distributions in the LHC era: MMHT 2014 PDFs*, *Eur. Phys. J.* **C 75** (2015) 204 [arXiv:1412.3989] [INSPIRE].

[42] NNPDF collaboration, R.D. Ball et al., *Parton distributions for the LHC Run II*, *JHEP* **04** (2015) 040 [arXiv:1410.8849] [INSPIRE].

[43] K. Hamilton, P. Nason, E. Re and G. Zanderighi, *NNLOPS simulation of Higgs boson production*, *JHEP* **10** (2013) 222 [arXiv:1309.0017] [INSPIRE].

[44] LHCb collaboration, *Measurement of the forward-backward asymmetry in $Z/\gamma^* \to \mu^+ \mu^-$ decays and determination of the effective weak mixing angle*, *JHEP* **11** (2015) 190 [arXiv:1509.07645] [INSPIRE].

[45] LHCb collaboration, *Inclusive W and Z production in the forward region at $\sqrt{s} = 7\,TeV$*, *JHEP* **06** (2012) 058 [arXiv:1204.1620] [INSPIRE].

[46] M. Bahr et al., *HERWIG++ Physics and Manual*, *Eur. Phys. J.* **C 58** (2008) 639 [arXiv:0803.0883] [INSPIRE].

[47] T. Adye, *Unfolding algorithms and tests using RooUnfold*, arXiv:1105.1160 [INSPIRE].

[48] G. D'Agostini, *A Multidimensional unfolding method based on Bayes' theorem*, *Nucl. Instrum. Meth.* **A 362** (1995) 487 [INSPIRE].

[49] A. Hocker and V. Kartvelishvili, *SVD approach to data unfolding*, *Nucl. Instrum. Meth.* **A 372** (1996) 469 [hep-ph/9509307] [INSPIRE].

[50] G. Cowan, *Statistical Data Analysis*, Oxford University Press, (1998).

[51] P. Nason, *A new method for combining NLO QCD with shower Monte Carlo algorithms*, *JHEP* **11** (2004) 040 [hep-ph/0409146] [INSPIRE].

[52] S. Frixione, P. Nason and C. Oleari, *Matching NLO QCD computations with Parton Shower simulations: the POWHEG method*, *JHEP* **11** (2007) 070 [arXiv:0709.2092] [INSPIRE].

[53] S. Alioli, P. Nason, C. Oleari and E. Re, *A general framework for implementing NLO calculations in shower Monte Carlo programs: the POWHEG BOX*, *JHEP* **06** (2010) 043 [arXiv:1002.2581] [INSPIRE].

[54] J. Wenninger,, *Energy Calibration of the LHC Beams at 4 TeV*, CERN-ATS-2013-040, CERN, (2013).

[55] S. Catani, L. Cieri, G. Ferrera, D. de Florian and M. Grazzini, *Vector boson production at hadron colliders: A fully exclusive QCD calculation at NNLO*, *Phys. Rev. Lett.* **103** (2009) 082001 [arXiv:0903.2120] [INSPIRE].

[56] R. Nisius, *On the combination of correlated estimates of a physics observable*, *Eur. Phys. J.* **C 74** (2014) 3004 [arXiv:1402.4016] [INSPIRE].

The LHCb collaboration

R. Aaij[39], C. Abellán Beteta[41], B. Adeva[38], M. Adinolfi[47], A. Affolder[53], Z. Ajaltouni[5], S. Akar[6],
J. Albrecht[10], F. Alessio[39], M. Alexander[52], S. Ali[42], G. Alkhazov[31], P. Alvarez Cartelle[54],
A.A. Alves Jr[58], S. Amato[2], S. Amerio[23], Y. Amhis[7], L. An[3,40], L. Anderlini[18], G. Andreassi[40],
M. Andreotti[17,g], J.E. Andrews[59], R.B. Appleby[55], O. Aquines Gutierrez[11], F. Archilli[39],
P. d'Argent[12], A. Artamonov[36], M. Artuso[60], E. Aslanides[6], G. Auriemma[26,n], M. Baalouch[5],
S. Bachmann[12], J.J. Back[49], A. Badalov[37], C. Baesso[61], W. Baldini[17,39], R.J. Barlow[55],
C. Barschel[39], S. Barsuk[7], W. Barter[39], V. Batozskaya[29], V. Battista[40], A. Bay[40], L. Beaucourt[4],
J. Beddow[52], F. Bedeschi[24], I. Bediaga[1], L.J. Bel[42], V. Bellee[40], N. Belloli[21,k], I. Belyaev[32],
E. Ben-Haim[8], G. Bencivenni[19], S. Benson[39], J. Benton[47], A. Berezhnoy[33], R. Bernet[41],
A. Bertolin[23], M.-O. Bettler[39], M. van Beuzekom[42], S. Bifani[46], P. Billoir[8], T. Bird[55],
A. Birnkraut[10], A. Bizzeti[18,i], T. Blake[49], F. Blanc[40], J. Blouw[11], S. Blusk[60], V. Bocci[26],
A. Bondar[35], N. Bondar[31,39], W. Bonivento[16], S. Borghi[55], M. Borisyak[66], M. Borsato[38],
T.J.V. Bowcock[53], E. Bowen[41], C. Bozzi[17,39], S. Braun[12], M. Britsch[12], T. Britton[60],
J. Brodzicka[55], N.H. Brook[47], E. Buchanan[47], C. Burr[55], A. Bursche[41], J. Buytaert[39],
S. Cadeddu[16], R. Calabrese[17,g], M. Calvi[21,k], M. Calvo Gomez[37,p], P. Campana[19],
D. Campora Perez[39], L. Capriotti[55], A. Carbone[15,e], G. Carboni[25,l], R. Cardinale[20,j],
A. Cardini[16], P. Carniti[21,k], L. Carson[51], K. Carvalho Akiba[2], G. Casse[53], L. Cassina[21,k],
L. Castillo Garcia[40], M. Cattaneo[39], Ch. Cauet[10], G. Cavallero[20], R. Cenci[24,t], M. Charles[8],
Ph. Charpentier[39], M. Chefdeville[4], S. Chen[55], S.-F. Cheung[56], N. Chiapolini[41],
M. Chrzaszcz[41,27], X. Cid Vidal[39], G. Ciezarek[42], P.E.L. Clarke[51], M. Clemencic[39], H.V. Cliff[48],
J. Closier[39], V. Coco[39], J. Cogan[6], E. Cogneras[5], V. Cogoni[16,f], L. Cojocariu[30], G. Collazuol[23,r],
P. Collins[39], A. Comerma-Montells[12], A. Contu[39], A. Cook[47], M. Coombes[47], S. Coquereau[8],
G. Corti[39], M. Corvo[17,g], B. Couturier[39], G.A. Cowan[51], D.C. Craik[51], A. Crocombe[49],
M. Cruz Torres[61], S. Cunliffe[54], R. Currie[54], C. D'Ambrosio[39], E. Dall'Occo[42], J. Dalseno[47],
P.N.Y. David[42], A. Davis[58], O. De Aguiar Francisco[2], K. De Bruyn[6], S. De Capua[55],
M. De Cian[12], J.M. De Miranda[1], L. De Paula[2], P. De Simone[19], C.-T. Dean[52], D. Decamp[4],
M. Deckenhoff[10], L. Del Buono[8], N. Déléage[4], M. Demmer[10], D. Derkach[66], O. Deschamps[5],
F. Dettori[39], B. Dey[22], A. Di Canto[39], F. Di Ruscio[25], H. Dijkstra[39], S. Donleavy[53], F. Dordei[39],
M. Dorigo[40], A. Dosil Suárez[38], A. Dovbnya[44], K. Dreimanis[53], L. Dufour[42], G. Dujany[55],
K. Dungs[39], P. Durante[39], R. Dzhelyadin[36], A. Dziurda[27], A. Dzyuba[31], S. Easo[50,39], U. Egede[54],
V. Egorychev[32], S. Eidelman[35], S. Eisenhardt[51], U. Eitschberger[10], R. Ekelhof[10], L. Eklund[52],
I. El Rifai[5], Ch. Elsasser[41], S. Ely[60], S. Esen[12], H.M. Evans[48], T. Evans[56], M. Fabianska[27],
A. Falabella[15], C. Färber[39], N. Farley[46], S. Farry[53], R. Fay[53], D. Ferguson[51],
V. Fernandez Albor[38], F. Ferrari[15], F. Ferreira Rodrigues[1], M. Ferro-Luzzi[39], S. Filippov[34],
M. Fiore[17,39,g], M. Fiorini[17,g], M. Firlej[28], C. Fitzpatrick[40], T. Fiutowski[28], F. Fleuret[7,b],
K. Fohl[39], P. Fol[54], M. Fontana[16], F. Fontanelli[20,j], D. C. Forshaw[60], R. Forty[39], M. Frank[39],
C. Frei[39], M. Frosini[18], J. Fu[22], E. Furfaro[25,l], A. Gallas Torreira[38], D. Galli[15,e], S. Gallorini[23],
S. Gambetta[51], M. Gandelman[2], P. Gandini[56], Y. Gao[3], J. García Pardiñas[38], J. Garra Tico[48],
L. Garrido[37], D. Gascon[37], C. Gaspar[39], R. Gauld[56], L. Gavardi[10], G. Gazzoni[5], D. Gerick[12],
E. Gersabeck[12], M. Gersabeck[55], T. Gershon[49], Ph. Ghez[4], S. Gianì[40], V. Gibson[48],
O.G. Girard[40], L. Giubega[30], V.V. Gligorov[39], C. Göbel[61], D. Golubkov[32], A. Golutvin[54,39],
A. Gomes[1,a], C. Gotti[21,k], M. Grabalosa Gándara[5], R. Graciani Diaz[37], L.A. Granado Cardoso[39],
E. Graugés[37], E. Graverini[41], G. Graziani[18], A. Grecu[30], E. Greening[56], P. Griffith[46], L. Grillo[12],
O. Grünberg[64], B. Gui[60], E. Gushchin[34], Yu. Guz[36,39], T. Gys[39], T. Hadavizadeh[56],
C. Hadjivasiliou[60], G. Haefeli[40], C. Haen[39], S.C. Haines[48], S. Hall[54], B. Hamilton[59], X. Han[12],
S. Hansmann-Menzemer[12], N. Harnew[56], S.T. Harnew[47], J. Harrison[55], J. He[39], T. Head[40],

V. Heijne[42], A. Heister[9], K. Hennessy[53], P. Henrard[5], L. Henry[8], J.A. Hernando Morata[38],
E. van Herwijnen[39], M. Heß[64], A. Hicheur[2], D. Hill[56], M. Hoballah[5], C. Hombach[55],
W. Hulsbergen[42], T. Humair[54], M. Hushchyn[66], N. Hussain[56], D. Hutchcroft[53], D. Hynds[52],
M. Idzik[28], P. Ilten[57], R. Jacobsson[39], A. Jaeger[12], J. Jalocha[56], E. Jans[42], A. Jawahery[59],
M. John[56], D. Johnson[39], C.R. Jones[48], C. Joram[39], B. Jost[39], N. Jurik[60], S. Kandybei[44],
W. Kanso[6], M. Karacson[39], T.M. Karbach[39,†], S. Karodia[52], M. Kecke[12], M. Kelsey[60],
I.R. Kenyon[46], M. Kenzie[39], T. Ketel[43], E. Khairullin[66], B. Khanji[21,39,k], C. Khurewathanakul[40],
T. Kirn[9], S. Klaver[55], K. Klimaszewski[29], O. Kochebina[7], M. Kolpin[12], I. Komarov[40],
R.F. Koopman[43], P. Koppenburg[42,39], P. Krokovny[35], F. Kruse[10], W. Krzemien[29], W. Kucewicz[27,o], M. Kucharczyk[27],
V. Kudryavtsev[35], A. K. Kuonen[40], K. Kurek[29], T. Kvaratskheliya[32], D. Lacarrere[39],
G. Lafferty[55,39], A. Lai[16], D. Lambert[51], G. Lanfranchi[19], C. Langenbruch[49], B. Langhans[39],
T. Latham[49], C. Lazzeroni[46], R. Le Gac[6], J. van Leerdam[42], J.-P. Lees[4], R. Lefèvre[5],
A. Leflat[33,39], J. Lefrançois[7], E. Lemos Cid[38], O. Leroy[6], T. Lesiak[27], B. Leverington[12], Y. Li[7],
T. Likhomanenko[66,65], M. Liles[53], R. Lindner[39], C. Linn[39], F. Lionetto[41], B. Liu[16], X. Liu[3],
D. Loh[49], I. Longstaff[52], J.H. Lopes[2], D. Lucchesi[23,r], M. Lucio Martinez[38], H. Luo[51],
A. Lupato[23], E. Luppi[17,g], O. Lupton[56], A. Lusiani[24], F. Machefert[7], F. Maciuc[30], O. Maev[31],
K. Maguire[55], S. Malde[56], A. Malinin[65], G. Manca[7], G. Mancinelli[6], P. Manning[60], A. Mapelli[39],
J. Maratas[5], J.F. Marchand[4], U. Marconi[15], C. Marin Benito[37], P. Marino[24,39,t], J. Marks[12],
G. Martellotti[26], M. Martin[6], M. Martinelli[40], D. Martinez Santos[38], F. Martinez Vidal[67],
D. Martins Tostes[2], L.M. Massacrier[7], A. Massafferri[1], R. Matev[39], A. Mathad[49], Z. Mathe[39],
C. Matteuzzi[21], A. Mauri[41], B. Maurin[40], A. Mazurov[46], M. McCann[54], J. McCarthy[46],
A. McNab[55], R. McNulty[13], B. Meadows[58], F. Meier[10], M. Meissner[12], D. Melnychuk[29],
M. Merk[42], E Michielin[23], D.A. Milanes[63], M.-N. Minard[4], D.S. Mitzel[12], J. Molina Rodriguez[61],
I.A. Monroy[63], S. Monteil[5], M. Morandin[23], P. Morawski[28], A. Mordà[6], M.J. Morello[24,t],
J. Moron[28], A.B. Morris[51], R. Mountain[60], F. Muheim[51], D. Müller[55], J. Müller[10], K. Müller[41],
V. Müller[10], M. Mussini[15], B. Muster[40], P. Naik[47], T. Nakada[40], R. Nandakumar[50], A. Nandi[56],
I. Nasteva[2], M. Needham[51], N. Neri[22], S. Neubert[12], N. Neufeld[39], M. Neuner[12], A.D. Nguyen[40],
T.D. Nguyen[40], C. Nguyen-Mau[40,q], V. Niess[5], R. Niet[10], N. Nikitin[33], T. Nikodem[12],
A. Novoselov[36], D.P. O'Hanlon[49], A. Oblakowska-Mucha[28], V. Obraztsov[36], S. Ogilvy[52],
O. Okhrimenko[45], R. Oldeman[16,f], C.J.G. Onderwater[68], B. Osorio Rodrigues[1],
J.M. Otalora Goicochea[2], A. Otto[39], P. Owen[54], A. Oyanguren[67], A. Palano[14,d], F. Palombo[22,u],
M. Palutan[19], J. Panman[39], A. Papanestis[50], M. Pappagallo[52], L.L. Pappalardo[17,g],
C. Pappenheimer[58], W. Parker[59], C. Parkes[55], G. Passaleva[18], G.D. Patel[53], M. Patel[54],
C. Patrignani[20,j], A. Pearce[55,50], A. Pellegrino[42], G. Penso[26,m], M. Pepe Altarelli[39],
S. Perazzini[15,e], P. Perret[5], L. Pescatore[46], K. Petridis[47], A. Petrolini[20,j], M. Petruzzo[22],
E. Picatoste Olloqui[37], B. Pietrzyk[4], M. Pikies[27], D. Pinci[26], A. Pistone[20], A. Piucci[12],
S. Playfer[51], M. Plo Casasus[38], T. Poikela[39], F. Polci[8], A. Poluektov[49,35], I. Polyakov[32],
E. Polycarpo[2], A. Popov[36], D. Popov[11,39], B. Popovici[30], C. Potterat[2], E. Price[47], J.D. Price[53],
J. Prisciandaro[38], A. Pritchard[53], C. Prouve[47], V. Pugatch[45], A. Puig Navarro[40], G. Punzi[24,s],
W. Qian[4], R. Quagliani[7,47], B. Rachwal[27], J.H. Rademacker[47], M. Rama[24], M. Ramos Pernas[38],
M.S. Rangel[2], I. Raniuk[44], N. Rauschmayr[39], G. Raven[43], F. Redi[54], S. Reichert[55],
A.C. dos Reis[1], V. Renaudin[7], S. Ricciardi[50], S. Richards[47], M. Rihl[39], K. Rinnert[53,39],
V. Rives Molina[37], P. Robbe[7,39], A.B. Rodrigues[1], E. Rodrigues[55], J.A. Rodriguez Lopez[63],
P. Rodriguez Perez[55], S. Roiser[39], V. Romanovsky[36], A. Romero Vidal[38], J. W. Ronayne[13],
M. Rotondo[23], T. Ruf[39], P. Ruiz Valls[67], J.J. Saborido Silva[38], N. Sagidova[31], B. Saitta[16,f],
V. Salustino Guimaraes[2], C. Sanchez Mayordomo[67], B. Sanmartin Sedes[38], R. Santacesaria[26],
C. Santamarina Rios[38], M. Santimaria[19], E. Santovetti[25,l], A. Sarti[19,m], C. Satriano[26,n],

A. Satta[25], D.M. Saunders[47], D. Savrina[32,33], S. Schael[9], M. Schiller[39], H. Schindler[39],
M. Schlupp[10], M. Schmelling[11], T. Schmelzer[10], B. Schmidt[39], O. Schneider[40], A. Schopper[39],
M. Schubiger[40], M.-H. Schune[7], R. Schwemmer[39], B. Sciascia[19], A. Sciubba[26,m], A. Semennikov[32],
A. Sergi[46], N. Serra[41], J. Serrano[6], L. Sestini[23], P. Seyfert[21], M. Shapkin[36], I. Shapoval[17,44,g],
Y. Shcheglov[31], T. Shears[53], L. Shekhtman[35], V. Shevchenko[65], A. Shires[10], B.G. Siddi[17],
R. Silva Coutinho[41], L. Silva de Oliveira[2], G. Simi[23,s], M. Sirendi[48], N. Skidmore[47],
T. Skwarnicki[60], E. Smith[56,50], E. Smith[54], I.T. Smith[51], J. Smith[48], M. Smith[55], H. Snoek[42],
M.D. Sokoloff[58,39], F.J.P. Soler[52], F. Soomro[40], D. Souza[47], B. Souza De Paula[2], B. Spaan[10],
P. Spradlin[52], S. Sridharan[39], F. Stagni[39], M. Stahl[12], S. Stahl[39], S. Stefkova[54], O. Steinkamp[41],
O. Stenyakin[36], S. Stevenson[56], S. Stoica[30], S. Stone[60], B. Storaci[41], S. Stracka[24,t],
M. Straticiuc[30], U. Straumann[41], L. Sun[58], W. Sutcliffe[54], K. Swientek[28], S. Swientek[10],
V. Syropoulos[43], M. Szczekowski[29], T. Szumlak[28], S. T'Jampens[4], A. Tayduganov[6],
T. Tekampe[10], G. Tellarini[17,g], F. Teubert[39], C. Thomas[56], E. Thomas[39], J. van Tilburg[42],
V. Tisserand[4], M. Tobin[40], J. Todd[58], S. Tolk[43], L. Tomassetti[17,g], D. Tonelli[39],
S. Topp-Joergensen[56], N. Torr[56], E. Tournefier[4], S. Tourneur[40], K. Trabelsi[40], M. Traill[52],
M.T. Tran[40], M. Tresch[41], A. Trisovic[39], A. Tsaregorodtsev[6], P. Tsopelas[42], N. Tuning[42,39],
A. Ukleja[29], A. Ustyuzhanin[66,65], U. Uwer[12], C. Vacca[16,39,f], V. Vagnoni[15], G. Valenti[15],
A. Vallier[7], R. Vazquez Gomez[19], P. Vazquez Regueiro[38], C. Vázquez Sierra[38], S. Vecchi[17],
M. van Veghel[43], J.J. Velthuis[47], M. Veltri[18,h], G. Veneziano[40], M. Vesterinen[12], B. Viaud[7],
D. Vieira[2], M. Vieites Diaz[38], X. Vilasis-Cardona[37,p], V. Volkov[33], A. Vollhardt[41], D. Voong[47],
A. Vorobyev[31], V. Vorobyev[35], C. Voß[64], J.A. de Vries[42], R. Waldi[64], C. Wallace[49], R. Wallace[13],
J. Walsh[24], J. Wang[60], D.R. Ward[48], N.K. Watson[46], D. Websdale[54], A. Weiden[41],
M. Whitehead[39], J. Wicht[49], G. Wilkinson[56,39], M. Wilkinson[60], M. Williams[39], M.P. Williams[46],
M. Williams[57], T. Williams[46], F.F. Wilson[50], J. Wimberley[59], J. Wishahi[10], W. Wislicki[29],
M. Witek[27], G. Wormser[7], S.A. Wotton[48], K. Wraight[52], S. Wright[48], K. Wyllie[39], Y. Xie[62],
Z. Xu[40], Z. Yang[3], J. Yu[62], X. Yuan[35], O. Yushchenko[36], M. Zangoli[15], M. Zavertyaev[11,c],
L. Zhang[3], Y. Zhang[3], A. Zhelezov[12], A. Zhokhov[32], L. Zhong[3], V. Zhukov[9], S. Zucchelli[15].

1   Centro Brasileiro de Pesquisas Físicas (CBPF), Rio de Janeiro, Brazil
2   Universidade Federal do Rio de Janeiro (UFRJ), Rio de Janeiro, Brazil
3   Center for High Energy Physics, Tsinghua University, Beijing, China
4   LAPP, Université Savoie Mont-Blanc, CNRS/IN2P3, Annecy-Le-Vieux, France
5   Clermont Université, Université Blaise Pascal, CNRS/IN2P3, LPC, Clermont-Ferrand, France
6   CPPM, Aix-Marseille Université, CNRS/IN2P3, Marseille, France
7   LAL, Université Paris-Sud, CNRS/IN2P3, Orsay, France
8   LPNHE, Université Pierre et Marie Curie, Université Paris Diderot, CNRS/IN2P3, Paris, France
9   I. Physikalisches Institut, RWTH Aachen University, Aachen, Germany
10 Fakultät Physik, Technische Universität Dortmund, Dortmund, Germany
11 Max-Planck-Institut für Kernphysik (MPIK), Heidelberg, Germany
12 Physikalisches Institut, Ruprecht-Karls-Universität Heidelberg, Heidelberg, Germany
13 School of Physics, University College Dublin, Dublin, Ireland
14 Sezione INFN di Bari, Bari, Italy
15 Sezione INFN di Bologna, Bologna, Italy
16 Sezione INFN di Cagliari, Cagliari, Italy
17 Sezione INFN di Ferrara, Ferrara, Italy
18 Sezione INFN di Firenze, Firenze, Italy
19 Laboratori Nazionali dell'INFN di Frascati, Frascati, Italy
20 Sezione INFN di Genova, Genova, Italy
21 Sezione INFN di Milano Bicocca, Milano, Italy
22 Sezione INFN di Milano, Milano, Italy

JHEP01 (2016) 155

[23] *Sezione INFN di Padova, Padova, Italy*

[24] *Sezione INFN di Pisa, Pisa, Italy*

[25] *Sezione INFN di Roma Tor Vergata, Roma, Italy*

[26] *Sezione INFN di Roma La Sapienza, Roma, Italy*

[27] *Henryk Niewodniczanski Institute of Nuclear Physics Polish Academy of Sciences, Kraków, Poland*

[28] *AGH - University of Science and Technology, Faculty of Physics and Applied Computer Science, Kraków, Poland*

[29] *National Center for Nuclear Research (NCBJ), Warsaw, Poland*

[30] *Horia Hulubei National Institute of Physics and Nuclear Engineering, Bucharest-Magurele, Romania*

[31] *Petersburg Nuclear Physics Institute (PNPI), Gatchina, Russia*

[32] *Institute of Theoretical and Experimental Physics (ITEP), Moscow, Russia*

[33] *Institute of Nuclear Physics, Moscow State University (SINP MSU), Moscow, Russia*

[34] *Institute for Nuclear Research of the Russian Academy of Sciences (INR RAN), Moscow, Russia*

[35] *Budker Institute of Nuclear Physics (SB RAS) and Novosibirsk State University, Novosibirsk, Russia*

[36] *Institute for High Energy Physics (IHEP), Protvino, Russia*

[37] *Universitat de Barcelona, Barcelona, Spain*

[38] *Universidad de Santiago de Compostela, Santiago de Compostela, Spain*

[39] *European Organization for Nuclear Research (CERN), Geneva, Switzerland*

[40] *Ecole Polytechnique Fédérale de Lausanne (EPFL), Lausanne, Switzerland*

[41] *Physik-Institut, Universität Zürich, Zürich, Switzerland*

[42] *Nikhef National Institute for Subatomic Physics, Amsterdam, The Netherlands*

[43] *Nikhef National Institute for Subatomic Physics and VU University Amsterdam, Amsterdam, The Netherlands*

[44] *NSC Kharkiv Institute of Physics and Technology (NSC KIPT), Kharkiv, Ukraine*

[45] *Institute for Nuclear Research of the National Academy of Sciences (KINR), Kyiv, Ukraine*

[46] *University of Birmingham, Birmingham, United Kingdom*

[47] *H.H. Wills Physics Laboratory, University of Bristol, Bristol, United Kingdom*

[48] *Cavendish Laboratory, University of Cambridge, Cambridge, United Kingdom*

[49] *Department of Physics, University of Warwick, Coventry, United Kingdom*

[50] *STFC Rutherford Appleton Laboratory, Didcot, United Kingdom*

[51] *School of Physics and Astronomy, University of Edinburgh, Edinburgh, United Kingdom*

[52] *School of Physics and Astronomy, University of Glasgow, Glasgow, United Kingdom*

[53] *Oliver Lodge Laboratory, University of Liverpool, Liverpool, United Kingdom*

[54] *Imperial College London, London, United Kingdom*

[55] *School of Physics and Astronomy, University of Manchester, Manchester, United Kingdom*

[56] *Department of Physics, University of Oxford, Oxford, United Kingdom*

[57] *Massachusetts Institute of Technology, Cambridge, MA, United States*

[58] *University of Cincinnati, Cincinnati, OH, United States*

[59] *University of Maryland, College Park, MD, United States*

[60] *Syracuse University, Syracuse, NY, United States*

[61] *Pontifícia Universidade Católica do Rio de Janeiro (PUC-Rio), Rio de Janeiro, Brazil, associated to [2]*

[62] *Institute of Particle Physics, Central China Normal University, Wuhan, Hubei, China, associated to [3]*

[63] *Departamento de Fisica, Universidad Nacional de Colombia, Bogota, Colombia, associated to [8]*

[64] *Institut für Physik, Universität Rostock, Rostock, Germany, associated to [12]*

[65] *National Research Centre Kurchatov Institute, Moscow, Russia, associated to [32]*

[66] *Yandex School of Data Analysis, Moscow, Russia, associated to [32]*

[67] *Instituto de Fisica Corpuscular (IFIC), Universitat de Valencia-CSIC, Valencia, Spain, associated to [37]*

[68] *Van Swinderen Institute, University of Groningen, Groningen, The Netherlands, associated to [42]*

^{a} Universidade Federal do Triângulo Mineiro (UFTM), Uberaba-MG, Brazil

^{b} Laboratoire Leprince-Ringuet, Palaiseau, France

^{c} P.N. Lebedev Physical Institute, Russian Academy of Science (LPI RAS), Moscow, Russia

^{d} Università di Bari, Bari, Italy

^{e} Università di Bologna, Bologna, Italy

^{f} Università di Cagliari, Cagliari, Italy

^{g} Università di Ferrara, Ferrara, Italy

^{h} Università di Urbino, Urbino, Italy

^{i} Università di Modena e Reggio Emilia, Modena, Italy

^{j} Università di Genova, Genova, Italy

^{k} Università di Milano Bicocca, Milano, Italy

^{l} Università di Roma Tor Vergata, Roma, Italy

^{m} Università di Roma La Sapienza, Roma, Italy

^{n} Università della Basilicata, Potenza, Italy

^{o} AGH - University of Science and Technology, Faculty of Computer Science, Electronics and Telecommunications, Kraków, Poland

^{p} LIFAELS, La Salle, Universitat Ramon Llull, Barcelona, Spain

^{q} Hanoi University of Science, Hanoi, Viet Nam

^{r} Università di Padova, Padova, Italy

^{s} Università di Pisa, Pisa, Italy

^{t} Scuola Normale Superiore, Pisa, Italy

^{u} Università degli Studi di Milano, Milano, Italy

† Deceased